HIGHLY SEASONAL AND PERENNIAL FLUVIAL FACIES: IMPLICATIONS FOR CLIMATIC CONTROL ON THE DOUGLAS CREEK AND PARACHUTE CREEK MEMBERS, GREEN RIVER FORMATION, SOUTHEASTERN UINTA BASIN, UTAH

by

Ryan D. Gall

A thesis submitted to the faculty of
The University of Utah
in partial fulfillment of the requirements for the degree of

Master of Science

in

Geology

Department of Geology and Geophysics

The University of Utah

May 2017

The University of Utah Graduate School

STATEMENT OF THESIS APPROVAL

The thesis of **Ryan D. Gall**

has been approved by the following supervisory committee members:

Lauren Birgenheier	, Chair	**11/01/2016**
		Date Approved
Michael Vanden Berg	, Member	**11/09/2016**
		Date Approved
Cari Johnson	, Member	**11/01/2016**
		Date Approved

and by **Thure Cerling** , Chair/Dean of

the Department/College/School of **Geology and Geophysics**

and by David B. Kieda, Dean of The Graduate School.

ABSTRACT

The early to middle Eocene Green River Formation consists of continental strata deposited in Laramide ponded basins in Utah, Colorado, and Wyoming. This study (1) documents fluvial and lacustrine strata from the Douglas Creek and Parachute Creek Members of the middle Green River Formation, southeastern Uinta Basin, Utah, and (2) uses new interpretations of the link between climate and fluvial sedimentary expression to interpret the terrestrial evolution of early Eocene climate. The stratigraphy was analyzed via outcrops along a 10 km transect in Main Canyon on the Tavaputs Plateau, and is divided into three distinct, stratigraphically separated depositional settings: (1) the lowermost Interval 1 is dominated by amalgamated sandstone channels that contain 70-100% upper flow regime sedimentary structures. The channels are interpreted to represent fluvial deposits controlled by a highly seasonal climate, where most deposition was limited to seasonal flooding events. (2) Interval 2 is dominated by alternating siliciclastic and carbonate lacustrine deposits, interpreted as local pulsed fluvial siliciclastic input into shallow Lake Uinta, and periods of fluvial quiescence represented by littoral carbonate deposition. (3) The uppermost Interval 3 is dominated by erosively-based, trough cross bedded sandstone channels interbedded with littoral lacustrine and deltaic deposits. The Interval 3 sandstone channels are interpreted as perennial fluvial deposits with relatively little variation in annual discharge, akin to modern humid-temperate fluvial systems. The stratigraphic transition from seasonally-controlled

(Interval 1) to perennial (Interval 3) fluvial deposits is interpreted to represent a fundamental shift in Eocene climate, from the peak hyperthermal regime of the Early Eocene Climatic Optimum (EECO) to a more stable post-EECO climate.

TABLE OF CONTENTS

LIST OF FIGURES

Figures

LIST OF TABLES

ACKNOWLEDGEMENTS

I would like to extend my gratitude first and foremost to Dr. Lauren Birgenheier for her guidance throughout my time at the University of Utah, and for providing the opportunity to complete this great field-based project. It was a pleasure working with Lauren, and I especially value the technical skillset and professionalism that Lauren helped me cultivate. I am also grateful to have learned from my supervisory committee members Michael Vanden Berg and Cari Johnson. Mike's thorough knowledge of Uinta Basin stratigraphy greatly aided this project, and I of course value those engaged microbialite discussions. And I thank Cari for her sharing her broad knowledge in basin analysis and for teaching some great classes that influenced this project. I also thank the faculty and staff in the G&G department that have helped me develop as a scientist and as a person during my time at the University of Utah.

Thorough appreciation is extended to my field assistants Jennifer Morris, Parker Archer, Shawn Moore, Ellen Rosencrans, and Elle Birgenheier. Thanks for enduring all forms of Uinta Basin weather and for "coping" with top pop 40 music during our long drives. And a second well-deserved shout out to Parker for his many hours spent processing samples, and for openly enjoying the same music as I do.

To the friends that I've made at the U, thanks for making Salt Lake City a stellar place to live and I look forward to reunions to shralp some pow in the Wasatch. To Aubry and Julia, thanks for keeping me sane via frequent trips to the wilderness, and cheers to

our late nights in the office. To my dog friend Elie, thank you for reminding me that life is now and may your days continue to include chasing mountain critters without consent. And certainly, to my family, thank you for providing me with unconditional support to chase some odd western dream.

INTRODUCTION

Perennial and ephemeral fluvial facies models are widely used to interpret ancient fluvial successions (Cant and Walker, 1976; Tunbridge, 1984; Abdullatif, 1989; Bridge, 1993; Hickin, 1993; Galloway and Hobday, 1996; Nichols and Fisher, 2007; Miall, 2013). However, recent study of modern sub-humid to semi-arid monsoonal fluvial systems indicates that perennial and ephemeral fluvial facies are not consistent with all river systems, nor are the associated facies models applicable to a significant portion of the rock record (Fielding et al., 2009, 2011; Plink-Björklund, 2015). Unique from the relatively continuous discharge of perennial rivers and from the sporadic flash flood-associated discharge of ephemeral rivers, modern sub-humid to semi-arid monsoonal fluvial systems experience extreme variation in annual discharge via distinct wet and dry seasons. Modern monsoonal wet seasons are characterized by intense rainfall spanning several months controlled by the annual migration of the ITCZ, and are when associated fluvial systems experience 80-90% of their annual discharge and comparable sediment transport rates (Leier et al., 2005; Wang and Ding, 2008; Henck et al., 2010; Plink-Björklund, 2015). During the dry season, however, minimal precipitation leads to exceptionally low base flow conditions and limited sediment transport (Henck et al., 2010; Plink-Björklund, 2015). These river systems have been termed as “flashy” to encapsulate profound variation in discharge (Fielding et al., 2009). Herein we refer to “flashy” monsoonal fluvial systems as “highly seasonal” fluvial systems to account for

the seasonally controlled discharge observed in modern systems and to avoid confusion with flashy discharge also observed in arid ephemeral systems.

Deposits of a modern highly seasonal fluvial system are detailed by Fielding et al. (2009). A single monsoonal flood in the Burdekin River in sub-humid NE Australia may deposit up to 5 m of sediment dominated by plane parallel lamination, low-angle lamination, convex-upward bedforms (antidunes), and scour and fill structures, interpreted as upper flow regime (UFR) structures deposited under Froude transcritical to supercritical velocities. The presence of climbing ripples and antidunes further indicates high sediment loads and high sediment fallout rates (Alexander et al., 1999; Plink-Björklund, 2015). Froude subcritical structures such as trough cross strata are minor, and barforms typically associated with fluvial systems are notably cryptic or absent. Historically, UFR structures have been regarded as having a low preservation potential as sediment becomes subsequently reworked in lower flow regime conditions; however, UFR structures are readily preserved in highly season rivers where flood stage flows decelerate faster than sediment can equilibrate (Alexander et al., 1999, 2001). Hydrographs from the Burdekin and other highly seasonal rivers exemplify this unique characteristic, which show rapid rises to peak floodstage velocities and subsequently decline at nearly the same rates (Alexander et al., 1999; Henck et al., 2010). The thick UFR-dominated sedimentary successions of the Burdekin remain largely preserved during the dry season when baseflow is minimal, although they are likely to be reworked by subsequent seasonal flooding (Fielding et al., 2009).

Few examples of highly seasonal fluvial systems are recognized in the rock record, but include the Pennsylvanian Sydney Mines Formation of Atlantic Canada, the

Eocene Wasatch Formation of Utah and Colorado, and parts of the Green River Formation in Utah (Fielding et al., 2009; Plink-Björklund, 2015). Recognition criteria for ancient highly seasonal fluvial deposits includes highly amalgamated, laterally-extensive and weakly-erosive channelized sandstone bodies that contain an abundance (50-100%) of UFR structures, lack of lateral accretion sets and well-developed macroforms, and subordinate current ripples and trough cross stratification (Fielding et al., 2009, 2011; Plink-Björklund, 2015). Amalgamated sandstone bodies represent multiple lateral and vertical stories that can be greater than 10 m thick (Fielding et al., 2011). Abrupt vertical and lateral transitions from channelized bodies to gray-to-red pedogenically-modified siltstone interbedded with overbank sandstone deposits characterizes the floodplain archetype of semi-arid to sub-humid highly seasonal fluvial systems (Fielding et al., 2009, 2011; Driese and Ober, 2005).

The aim of this study is to provide detailed documentation of highly seasonal fluvial deposits in addition to other fluvial and lacustrine strata from the Douglas Creek and Parachute Creek Members, Green River Formation (GRF), found in Main Canyon, Uinta Basin, Utah (Figure 1). Observations of highly seasonal fluvial deposits in Main Canyon expand the current facies model to include excellent preservation of well-developed downstream accreting macroforms and interbedded heterolithic channels. The study area also contains typical trough cross bedded perennial fluvial deposits that are stratigraphically separated from the highly seasonal example by a 60 m thick lacustrine-dominated interval, providing an avenue to document vertical trends of marginal Lake Uinta and compare fluvial depositional styles and controls. A secondary aim of this study is to assess the vertical trends in relation to the Early Eocene Climatic Optimum (EECO)

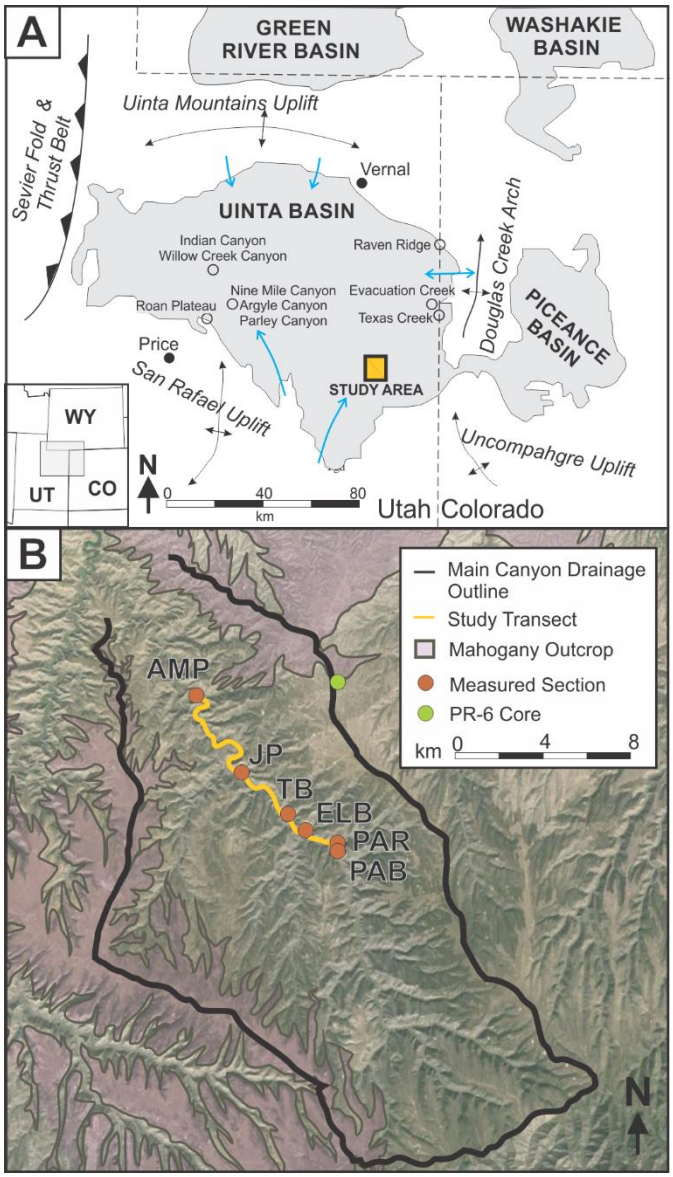

Figure 1. Map of the Uinta Basin and study area. A) Structural uplifts and basins containing Green River Formation with focus on Uinta Basin of Utah and Colorado. The Main Canyon study transect location is highlighted by the yellow square, with other Green River Formation, Uinta Basin study areas referenced in text denoted by open circles. AC, Argyle Canyon; EC, Evacuation Creek; IC, Indian Canyon; NMC, Nine Mile Canyon; PC, Parley Canyon; RP, Roan Plateau; RR, Raven Ridge; TC, Texas Creek; EC, Evacuation Creek. Blue arrows indicate dominant Eocene sediment transport direction from Smith et al. (2008), Davis et al. (2010), and this study. B) Main Canyon study area of southeastern Uinta Basin. Mahogany zone outcrop outline from Vanden Berg (2008).

and comment on whether the EECO can be identified from the sedimentology observed in Main Canyon.

Geologic Background

The GRF represents terminal sediment capture in Laramide basins in Utah and Colorado (Uinta and Piceance Basins, comprising Lake Uinta), and in Wyoming (Greater Green River Basin, Lake Gosuite) (Figure 1A; Dickinson et al., 1988). Well-known for its organic rich lacustrine deposits and excellent outcrop exposures, the GRF has been widely studied for its economic resources (Cashion, 1967; Johnson, 1985; Blackett, 1996; Vanden Berg, 2008; Johnson et al., 2011) and used to develop well-established models of lacustrine facies associations and lake-type classifications that have been applied broadly to ancient lacustrine successions (Carroll et al., 1999; Bohacs et al., 2000). The 25,000 km^2 Uinta Basin of eastern Utah and western Colorado contains fluvial and lacustrine deposits of Eocene Lake Uinta bounded by Laramide uplifts and the Sevier fold and thrust belt (Figure 1A; Osmond, 1964; Dickinson et al., 1988). To the east, the basin is contained by a north-trending anticline, the Douglas Creek Arch, which was breached by lake water in the early Eocene hydrologically connecting the Uinta Basin and the Piceance Basin of western Colorado (Figure 1A; Johnson, 1985; Keighly et al., 2003; Smith et al., 2008; Tänavsuu-Milkeviciene and Sarg, 2012). The GRF is up to 2100 m thick in the northern Uinta Basin depocenter and gradually thins across a shallow ramp (<5°) to the southern basin margins (Bradley, 1931; Abbott, 1957).

Main Canyon is located in southern Uintah County on the Tavaputs Plateau of the southeastern Uinta Basin (Figure 1B). Here and elsewhere across the southern Uinta

Basin, paleocurrent data indicate sediment was delivered from the south and originally thought to be largely sourced from local Laramide structures such as the San Rafael Swell and Uncompaghre Uplift, which may have continued to be active in the early Eocene (Osmond, 1964). However, recent provenance studies of the underlying and interfingering Eocene fluvial Wasatch Formation indicate that significant siliciclastic sediment likely originated 750 km away from the Uinta Basin in the Cordilleran arc of the Mojave region, California (Davis et al., 2010). While Wasatch Formation provenance is not indicative of sediment source of the GRF in the southern Uinta Basin, it suggests a large potential catchment area for Lake Uinta.

A plethora of names have been applied to lithostratigraphic subdivisions of the GRF and established terminology varies from the western and eastern Uinta Basin (Figure 2), a result of limited correlatable markers, few age constraints, and variable outcrop exposure (Keighley et al., 2003; Morgan et al., 2003). The lower GRF consists of carbonate deposition in a fresh to saline lake (Uteland Butte Limestone and Carbonate Marker Unit) punctuated by repeated fluvial re-expansion into the basin (the "Colton Tongue" of the Wasatch Fm) (Fouch, 1975; Pitman et al., 1982; Fouch et al., 1987). The middle GRF and focus of this study consists of the Douglas Creek and Parachute Creek Members of the eastern Uinta Basin, which overlies the Carbonate Marker Unit and records an overall expansion of saline Lake Uinta. The Douglas Creek Member is stratigraphically equivalent to the fluvial-deltaic and mouthbar facies of the Sunnyside Delta Interval of western Uinta Basin (Figure 2; Remy, 1992; Keighley et al., 2003; Taylor and Ritts, 2004; Schomacker et al., 2010; Moore et al., 2012), which contains three prominent carbonate marker beds (from base to top: C3, C2, and C1; Jacob, 1969).

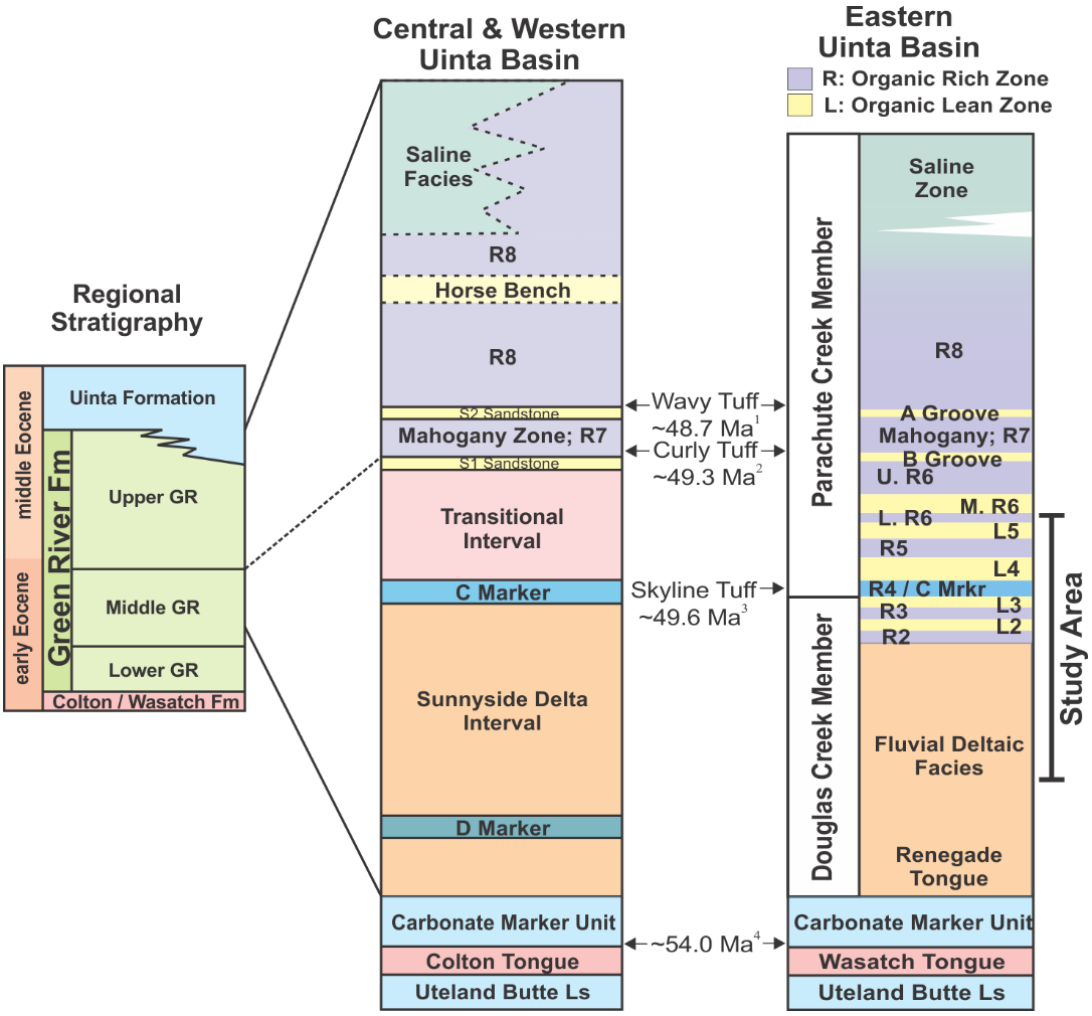

Figure 2. Generalized stratigraphy of the Green River Formation in the Uinta Basin. Age constraint references: [1]Smith et al. (2010); [2]Smith et al. (2008); [3]Smith and Carroll (2015); [4]Remy (1992). Stratigraphy references: Keighley et al. (2002), Cashion (1967), Morgan et al. (2003), Vanden Berg (2008), Remy (1992).

The C1 marker of Jacob (1969) is equivalent to the C-Marker of Remy (1992) that caps the Sunnyside Delta Interval and is identified in the eastern Uinta Basin in this study. Herein, the C-Marker is further correlated to the carbonate mudstone "R4" zone of the eastern Uinta and Piceance Basins based on sedimentology and relative stratigraphic thickness of carbonate units. The Parachute Creek Member is equivalent to the Transitional Interval of the western basin and represents the transition from fluvial-deltaic to lacustrine-dominated deposition. The basinwide Mahogany zone, an organic-rich carbonate mudstone, represents the height of Lake Uinta expansion and organic productivity marking the boundary between the middle and upper GRF (Figure 2; Johnson, 1985; Vanden Berg, 2008; Johnson et al., 2011). The upper GRF represents the closing of Lake Uinta with underfilled saline facies and is capped by the terrestrial Uinta Formation (Dane, 1954; Dyni, 1996; Vanden Berg et al., 2012; Vanden Berg and Birgenheier, accepted).

The timing of the Douglas Creek and Parachute Creek member deposition is constrained to 54.0-49.3 Ma (Figure 2) which overlaps with the EECO (ca. 52.6-50.1 Ma, Figure 3; Smith et al., 2014). The R4 boundary between the Douglas Creek and Parachute Creek Members has yielded conflicting $^{40}Ar/^{39}Ar$ dates: the Yellow tuff of the Piceance Basin is dated at 51.24 +/- 0.52 Ma (Smith, Carroll, and Singer, 2008) and was subsequently corrected to 51.55 +/- 0.54 Ma (Smith et al., 2010); however, it remains uncertain if this is correctly correlated to the R4 of the Uinta Basin. More recently, the Skyline tuff from the Uinta Basin indicates the R4 was deposited ~49.58 +/- 0.32 Ma (Smith and Carroll, 2015), which was selected as the most reliable date for use in this study.

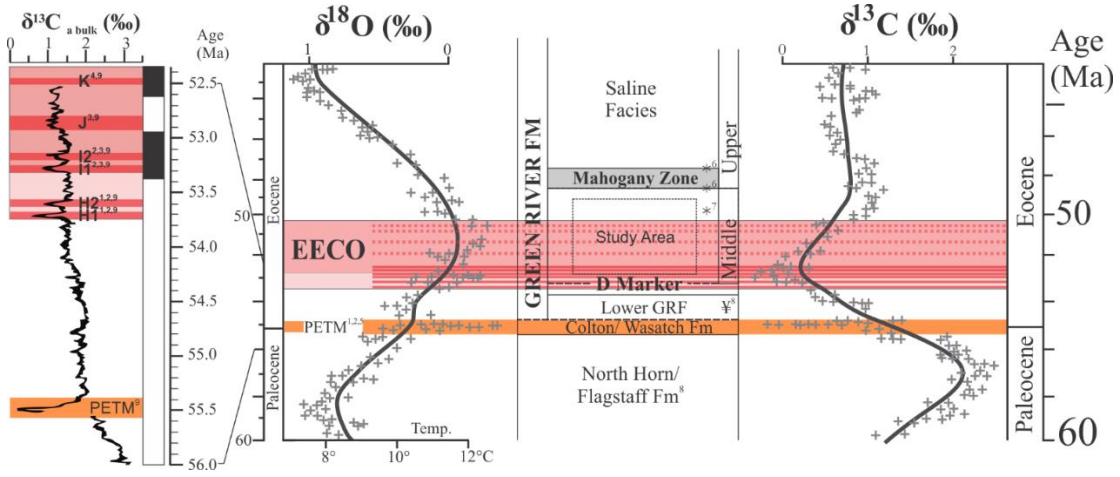

Figure 3. Paleogene isotopic records. Included is the Green River Formation stratigraphy using known age constraints, overlain on global climate-proxy records. Right: $\delta^{18}O$, paleotemperature, and $\delta^{13}C$ data from Zachos et al. (2001). Left: $\delta^{13}Ca$ bulk data from Zachos et al. (2010). Color designation: PETM (orange); established Early Eocene hyperthermal events (solid red lines: H1, H2, I1, I2, "J", "K"); lower magnitude, less well-studied Eocene hyperthermal (dotted red lines); period of active hyperthermal activity (pink); Early Eocene Climatic Optimum (dark pink). Age constraints: * dated tuff; ¥ base of Carbonate Marker Unit. References: [1]Lourens et al. (2006); [2]Nicolo et al. (2007); [3]Cramer et al. (2003); [4]Sexton et al. (2006); [5]Zachos et al. (2001); [6]Smith et al. (2010); [7]Smtih et al., (2015), [8]Remy (1992); [9]Zachos et al. (2010).

Eocene Climate

The EECO is characterized by repeated isotopic excursions from terrestrial and oceanic $\delta^{13}C$ and $\delta^{18}O$ records that followed the Paleocene-Eocene thermal Maximum (PETM) (Figure 3; Zachos et al., 2001, 2010; Cramer et al., 2003; Lourens et al., 2005; Smith et al., 2006, 2014; Nicolo et al., 2007; Hyland et al., 2013). At least eight isotopic excursions are recognized in the EECO, each interpreted as a short-duration period of drastically elevated atmospheric pCO^2 and rapid warming hyperthermal events (Zachos et al., 2001, 2010; Shellito et al., 2003; Lourens et al., 2005; Nicolo et al., 2007). Modeling results in conjunction with sedimentary records indicate the timing and reoccurrence of Eocene hyperthermal events coincide with 100 ky and 400 ky precessional and eccentricity cycles; however, a direct causation has yet to be proven (Clyde et al., 2001; Cramer et al., 2003; Lourens et al., 2005; Sexton et al., 2006; Zachos et al., 2010; Smith et al., 2014).

Isotopic, sedimentological, and paleontological evidence from terrestrial North America indicate rapid changes in temperature, precipitation, and biota throughout the EECO (e.g., Sewall and Sloan, 2006; Hren et al., 2010; Hyland et al., 2013). Climate proxy data from the adjacent Greater Green River Basin of Wyoming, for example, suggest significantly warmer (~7°C) and wetter (~750 mm yr^{-1}) hyperthermal conditions with concurrent floodplain deposits that suggest a semi-arid to sub-humid continental climate (Hyland and Sheldon, 2013). Further, western North America datasets indicate that Eocene hyperthermal events resulted in increased weathering rates (Smith et al., 2008; Hyland et al., 2013), expansion of fluvial systems (Abels et al., 2012; Smith et al.,

2014; Bataille et al., 2016), and likely resulted in alternating siliciclastic and carbonate deposition in lacustrine systems (Smith et al., 2014).

METHODS

Six stratigraphic sections totaling 762 m (AMP: 168 m; JP: 98 m; TB: 141 m; EB: 183 m; PAR: 124 m; PAB: 48 m) were measured across a 10 km NW-SE transect in Main Canyon (Figure 1B). Particular attention was paid to describing the sedimentology, sedimentary structures, trace fossils, paleoflow indicators, and bed geometries. Thin sections and XRD analyses (Appendix) were used to help determine lithofacies from fine-grained siliciclastic and carbonate rocks. Significant beds were walked out laterally and along cross cutting canyons to determine 3D relationships. Field measurements of fluvial channels were used in tandem with outcrop scape gigapans (automated high resolution photography and stitching) and detailed photomosaics (stitched photos) for architectural analysis. Architectural classification follows Ford and Pyles (2014) and is modified to include highly seasonal fluvial deposits (Figure 4).

Three carbonate marker beds can be laterally traced throughout field area and used to correlate sections across the 10 km transect (Figures 5, 6): 1) C-Marker, a 5-7 m thick accumulation of stacked white microbialite beds interbedded with wackestone and packstone, which is correlated to the C-Marker of Remy (1992) based on sedimentology; 2) Mass Transport (MT) Marker Bed, a 3-4 m thick vertically stacked debrite found in all measured sections except the northernmost AMP section; and 3) Upper Microbialite Marker, a 2-3 m thick interval consisting of three stacked brown microbialite beds interbedded with gray mudstone.

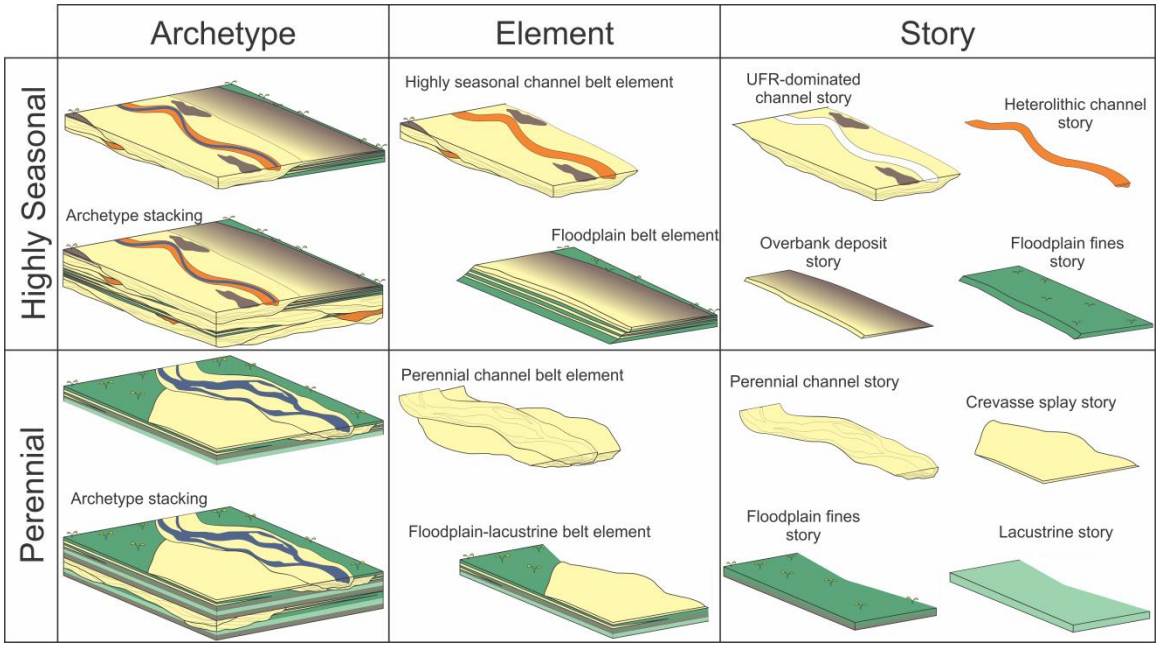

Figure 4. Architectural classification of fluvial deposits. Diagram includes highly seasonal (FA1.1, 1.2) and perennial (FA1.3) fluvial and associated deposits present in Main Canyon modeled after Ford and Pyles (2012).

Figure 5. Schematic stratigraphic section of Main Canyon. Stratigraphy is divided by interval with prominent marker beds and compiled paleocurrent data from the five measured sections. TS-A and TS-B correspond to Tar Sand zones A and B after Blackett (1996).

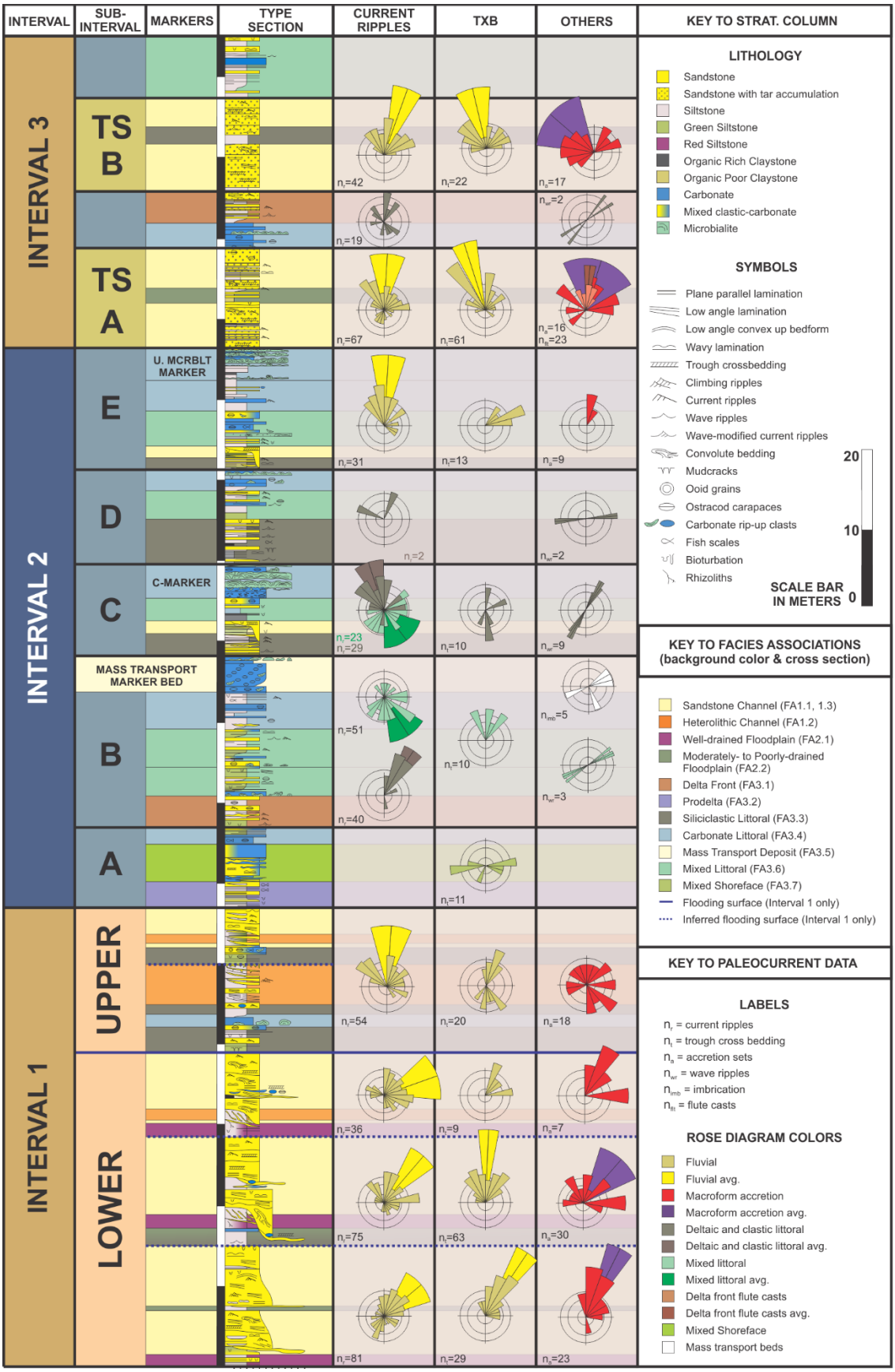
INTERVAL
SUB-INTERVAL
MARKERS
TYPE SECTION
CURRENT RIPPLES
TXB
OTHERS
KEY TO STRAT. COLUMN
INTERVAL 3
INTERVAL 2
INTERVAL 1
TS B
TS A
E
D
C
B
A
UPPER
LOWER
U. MCRBLT MARKER
C-MARKER
MASS TRANSPORT MARKER BED
LITHOLOGY
Sandstone
Sandstone with tar accumulation
Siltstone
Green Siltstone
Red Siltstone
Organic Rich Claystone
Organic Poor Claystone
Carbonate
Mixed clastic-carbonate
Microbialite
SYMBOLS
Plane parallel lamination
Low angle lamination
Low angle convex up bedform
Wavy lamination
Trough crossbedding
Climbing ripples
Current ripples
Wave ripples
Wave-modified current ripples
Convolute bedding
Mudcracks
Ooid grains
Ostracod carapaces
Carbonate rip-up clasts
Fish scales
Bioturbation
Rhizoliths
20
10
0
SCALE BAR IN METERS
KEY TO FACIES ASSOCIATIONS (background color & cross section)
Sandstone Channel (FA1.1, 1.3)
Heterolithic Channel (FA1.2)
Well-drained Floodplain (FA2.1)
Moderately- to Poorly-drained Floodplain (FA2.2)
Delta Front (FA3.1)
Prodelta (FA3.2)
Siliciclastic Littoral (FA3.3)
Carbonate Littoral (FA3.4)
Mass Transport Deposit (FA3.5)
Mixed Littoral (FA3.6)
Mixed Shoreface (FA3.7)
Flooding surface (Interval 1 only)
Inferred flooding surface (Interval 1 only)
KEY TO PALEOCURRENT DATA
LABELS
n_r = current ripples
n_t = trough cross bedding
n_a = accretion sets
n_{wr} = wave ripples
n_{imb} = imbrication
n_{fl} = flute casts
ROSE DIAGRAM COLORS
Fluvial
Fluvial avg.
Macroform accretion
Macroform accretion avg.
Deltaic and clastic littoral
Deltaic and clastic littoral avg.
Mixed littoral
Mixed littoral avg.
Delta front flute casts
Delta front flute casts avg.
Mixed Shoreface
Mass transport beds
n_r=42
n_t=22
n_a=17
n_{wr}=2
n_r=19
n_r=67
n_t=61
n_a=16
n_a=23
n_r=31
n_t=13
n_a=9
n_r=2
n_{wr}=2
n_r=23
n_r=29
n_t=10
n_{wr}=9
n_{imb}=5
n_r=51
n_t=10
n_r=40
n_{wr}=3
n_t=11
n_r=54
n_t=20
n_a=18
n_r=36
n_t=9
n_a=7
n_r=75
n_t=63
n_a=30
n_r=81
n_t=29
n_a=23

Figure 6. Diagrammatic correlation of measured sections and core. Measured section map locations shown in Fig 1B. The NW-SE cross section is oriented perpendicular to oblique to fluvial

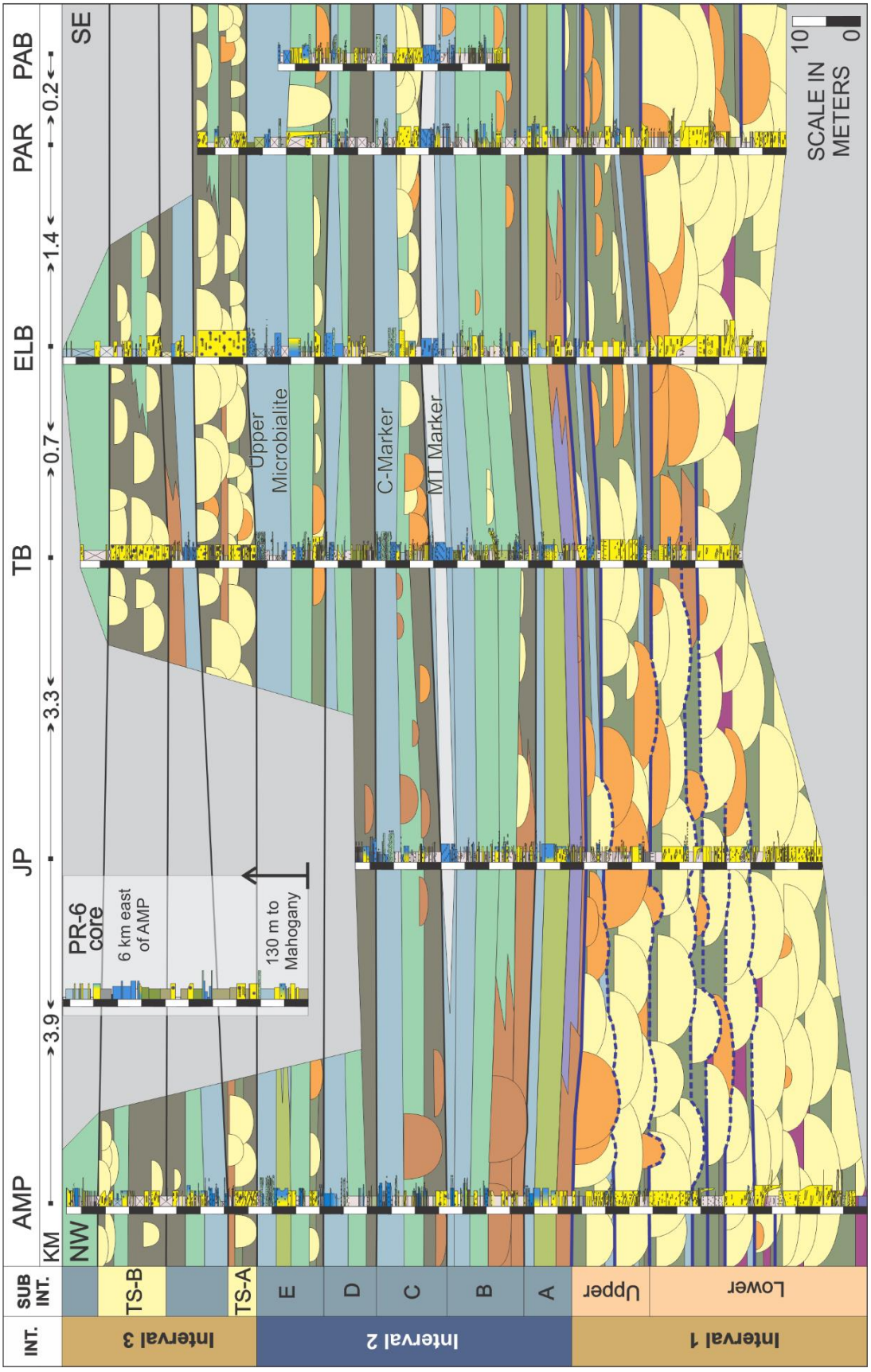
INT.
SUB INT.
KM
NW
AMP
JP
TB
ELB
PAR
PAB
SE
3.9
3.3
0.7
1.4
0.2
Interval 3
Interval 2
Interval 1
TS-B
TS-A
E
D
C
B
A
Upper
Lower
PR-6 core
6 km east of AMP
130 m to Mahogany
Upper Microbialite
C-Marker
MT Marker
SCALE IN METERS
10
0

To place the Main Canyon field area stratigraphically within a broader Uinta Basin context, sections were correlated to the PR-6 core taken six miles east of the northernmost section (Figures 1B, 6). The sedimentology of the PR-6 core was described at a centimeter scale at the Utah Geological Survey Core Research Center. The core was correlated to the field area based on sedimentology and the presence of a 4.5 m thick carbonate interval identified as the Upper Microbialite Marker and used to determine the stratigraphic distance of Main Canyon deposits from the Mahogany zone.

The measurement of laterally-extensive highly seasonal fluvial channel elements is confined to the lateral extent of outcrop exposures, which are limited by cross cutting canyons within the Main Canyon study area. For example, the largest measurable channel element on each gigapan is equal to the length of the outcrop exposure. Modern Main Canyon geomorphology is likely controlled to some extent by Eocene sandstone channel locations, although portions of many channels are eroded providing incomplete exposures. Care was taken to minimize error by only measuring elements with seemingly complete or nearly complete exposures and avoiding blatantly incomplete elements. The compiled fluvial element measurement data may be conservative for this reason, although it does not likely impact the overall interpretations put forth in this study.

FACIES ASSOCIATIONS

Fourteen lithofacies are identified in the Main Canyon field area, including five course-grained clastic facies (classified as S1 – S5), three fine-grained clastic facies (F1 – F3), two mixed clastic-carbonate facies (M1 – M2), and four carbonate facies (C1 – C4) (Table 1). Facies are grouped into 13 facies associations (Table 2) that span three main depositional settings: highly seasonal alluvial, perennial alluvial, and shallow lacustrine (Figure 7).

FA1.1 UFR-Dominated Fluvial Bodies

FA1.1 consists of low-angle lamination-dominated sandstone (S1) interbedded with gray mudstone (F1) that occurs within laterally-extensive lenticular bodies (Figures 8, 9). S1 is composed of very fine to medium sand and contains prominent internal lateral and vertical heterogeneity of sedimentary structures including low-angle lamination, low-angle convex-up bedforms, and plane parallel lamination, which are interpreted as UFR structures. Subordinate structures consist of climbing ripples, current ripples, trough cross stratification, convolute bedding, and flame structures. Trough cross bedding, where present, generally occurs at the base or near the top of an individual bed, though it can also be in the center of thick beds and bound vertically and laterally by low-angle lamination. Beds can exhibit slight normal grading. *Thalassinoides* burrows and

Table 1: Descriptions of lithofacies observed in the Main Canyon field area

ID	FACIES	DESCRIPTION	STRUCTURES*	GEOMETRY	PROCESSES
		Coarse-grained Clastics			
S1	LAL-dominated SST	Very fine to medium grained sandstone. Internal structures dominated by upper flow regime structures (60-100%). Flat to undulating base exhibit 0.1-5 m of erosive downcutting. Packages are highly amalgamated, and thin discontinuous mudstone beds can be found between amalgamated beds. *Thalassinoides* and iron concretions common at the top of individual beds. Mud clast inclusions and coarse-grained lag deposits are common, with minor inclusions of bone fragments, fish scales, and organic material. Large-scale accretion sets present.	PPL, LAL, LACU, ClR, CuR, SSD, M; minor TXB, flame structures	Lenticular to tabular; 0.1-4 m thick	Froude transcritical and supercritcal flow conditions
S2	TXB-dominated SST	Very fine to medium grained sandstone. Internal structures dominated by trough cross stratification (75-100%). Weakly-erosive to very-erosive bases with up to 10 m downcutting. Coarse grained lag deposits and accretion sets common. Minor fish scale and bone inclusions.	TXB, CuR, PPL, SSD; minor ClR	Lenticular; 0.2-2 m thick	Froude subcritical flow
S3	Massive tabular SST	Very fine to fine massive sandstone with sharp, non-erosive bases. Rare plane parallel lamination. Beds fine-upwards. Commonly calcareous with fish scales.	M, PPL	Tabular; 0.05-0.5 m thick	Unidirectional flow, turbidity currents
S4	Current rippled SST	Very fine to fine sandstone dominated by current ripples. Commonly normally graded. Bases are non-erosive to slightly erosive (<0.1 m).	CuR, M, LAL, PPl, ClR, minor TXB	Lenticular to tabular; 0.05-1 m thick	Unidirectional Froude subcritical flow
S5	Wave-rippled SST	Very fine to fine sandstone dominated by wave and wave-modified current ripples, with subordinate current ripples. Bases are non to slightly erosive (<5 cm).	WR, WmR	Tabular; 0.01-0.0.5 m thick	Oscillatory flow
		Fine-grained Clastics			
F1	Gray mudstone	Fissile claystone and siltstone. Most commonly organic-lean, with minor organic rich beds. Commonly gray, but can be gray-green, black, or brown. Commonly fines- or coarsens-upwards and is slope forming.	M, PPL, mud cracks, minor CuR, WR	Tabular, lenticular; 0.01-3 m thick	Suspension settling, traction currents
F2	Gray-green siltstone	Gray-green siltstone with blocky weathing pattern, and can grade into or is mottled purple. Commonly slightly calcareous with discontinuous, thin lentiicular sandstone beds. Root structures are common; mudcracks are present but rare. Packages commonly coarsen upwards.	M, mud cracks, rare rhizoliths	Tabular; 0.05-3 m thick	Settling of fine grains; reducing conditions

Table 1: Continued

ID	FACIES	DESCRIPTION	STRUCTURES*	GEOMETRY	PROCESSES
		Fine-grained Clastics			
F3	Red-tan siltstone	Tan-red, poorly-consolidated sandy siltstone. Mottled colors, root structures, calcite nodules, and ferrous nodules are common. Vertical, horizontal, and network burrow structures are common.	M, rhizoliths	Tabular; 0.2-3 m thick	Settling of fine grains; oxidation conditions
		Carbonate			
C1	Carbonate mudstone & wackestone	Carbonate mudstone and wackestone with spare ostracod and ooid grains. Usually organic poor; moderately-organic rich layers present.	M, WL	Tabular; 0.02-2 m thick	Precipitation followed by suspension settling
C2	Carbonate packstone & grainstone	Packstone and grainstone composed of ostracod and coated grains (ooids, pisoids, rare peloids). Carbonate mudstone or spar matrix. Beds non- to weakly-erosive.	M, WL, CuR	Lobate to tabular; 0.05-1 m thick	Unidirectional and oscillatory currents
C3	Microbialite	Microbialite facies that vary from discontinuous mats, isolated mounds, and laterally-extensive mound morphologies. Commonly contain ooid and ostracod grains within microbial fabric. Commonly diagenetically altered.	Microbialite fabrics	Mounds or tabular; 0.01-1 m thick	Microbially-induced carbonate production or grain capture
C4	Carbonate breccia	Poorly sorted, carbonate mud and ooid-grain supported carbonate conglomerate with carbonate mudstone and carbonate packstone rip-up clasts. Subrounded-subangular clasts are 1-5 cm wide, up to 0.5 cm thick, and slightly imbricated. Beds have weakly- to non-erosive bases.	M, imbricated clasts	Tabular; 0.1-2 m thick	Mass transport
		Mixed Clastic Carbonate			
M1	Laminated mixed	Mixed carbonate (ostracods, ooids, pisoids) and very fine to fine sand beds. Lamination and skolithios common.	PPL, LAL, CuR, WL	Lobate, tabular; 0.05-3 m thick	Unidirectional and oscillatory currents; traction deposition
M2	Massive mixed	Mixed carbonate (ostracods, ooids, pisoids) and very fine to medium sandstone beds, with isolated clasts up to 4 cm.	M, minor TXB, PPL, LAL	Tabular; 0.2-3 m thick	High energy reworking of sediment

*Sedimentary structure abbreviations: climbing ripples (ClR); current ripples (CuR); low-angle convex upward bedform (LACU); low-angle lamination (LAL); Massive (M); plane parallel lamination (PPL); soft sediment deformation (SSD); trough cross bedding (TXB); wavy lamination (WL); wave-modified current ripples (WmR); wave ripples (WR)

Table 2: Summary of facies assemblages and facie associations

FACIES ASSEMBLAGE	FACIES ASSOCIATION	ID	LITHOFACIES	INTERPRETATION
1 Fluvial	1.1 UFR-dominated fluvial bodies	S1	Low-angle lamination-dominated SST*	Seasonal fluvial flood deposits
		F1	Gray mudstone	Waning flow deposits, suspension settling
	1.2 Heterolithic fluvial bodies	S4	Current rippled SST	Perennial fluvial deposits
		F1	Gray mudstone	Low velocity deposition and inactive channel fill
		F2	Green-gray siltstone	Pedogenic modification of F1
		F3	Red-tan siltstone	Pedogenic modification of F1
	1.3 Trough cross bedded fluvial bodies	S2	Trough cross bedded SST	Froude subcritical fluvial deposition
		S3	Massive SST	Crevasse splay deposits
2 Floodplain	2.1 Well-drained floodplain	F3	Red-tan siltstone	Well-drained, oxidized paleosol
		S3	Massive SST	Overbank fluvial deposit
	2.2 Moderately- to poorly-drained floodplain	F2	Green-gray siltstone	Moderately-drained, reduced floodplain
		S3	Massive SST	Overbank fluvial deposit
3 Lacustrine	3.1 Delta front	F1	Gray mudstone	Suspension settling
		S4	Current rippled SST	Unidirectional fluvial input
		S5	Wave rippled SST	Oscillatory current reworking
	3.2 Prodelta	F1	Gray mudstone	Suspension settling
		S3	Massive SST	Turbidity flow driven accumulation
	3.3 Siliciclastic littoral	F1	Gray mudstone	Suspension settling
		F2	Green-gray mudstone	Marginal suspension settling; reducing conditions
		S4	Current rippled SST	Reworked sediment, clastic shoal
		S5	Wave rippled SST	Oscillatory current reworking
	3.4 Carbonate littoral	C1	Carbonate mudstone and wackestone	Suspension settling
		C2	Carbonate packstone and grainstone	Carbonate shoal and shoreface
		C3	Microbialites	Microbial carbonate precipitation and grain trapping
	3.5 Mass transport deposits	C4	Carbonate conglomerate	Mass transport beds

Table 2: Continued

FACIES ASSEMBLAGE	FACIES ASSOCIATION	ID	LITHOFACIES	INTERPRETATION
3 Lacustrine	3.6 Mixed littoral	M1	Laminated mixed	Reworked sediment; shoal
		M2	Massive mixed	Mixed shoal
		F1	Gray Mudstone	Suspension settling
		F2	Green-gray mudstone	Suspension settling, reduced setting
		S4	Current rippled SST	Clastic shoal
		S5	Wave rippled SST	Oscillatory current reworking
		C1	Carbonate mudstone and wackestone	Suspension settling
		C2	Carbonate packstone and grainstone	Carbonate shoal
		C3	Microbialites	Microbial carbonate precipitation and grain trapping
	3.7 Shoreface	C1	Carbonate mudstone and wackestone	Suspension settling, lower shoreface
		M2	Massive mixed	High energy, upper shoreface sediment reworking

*Sandstone abbreviated to "SST"

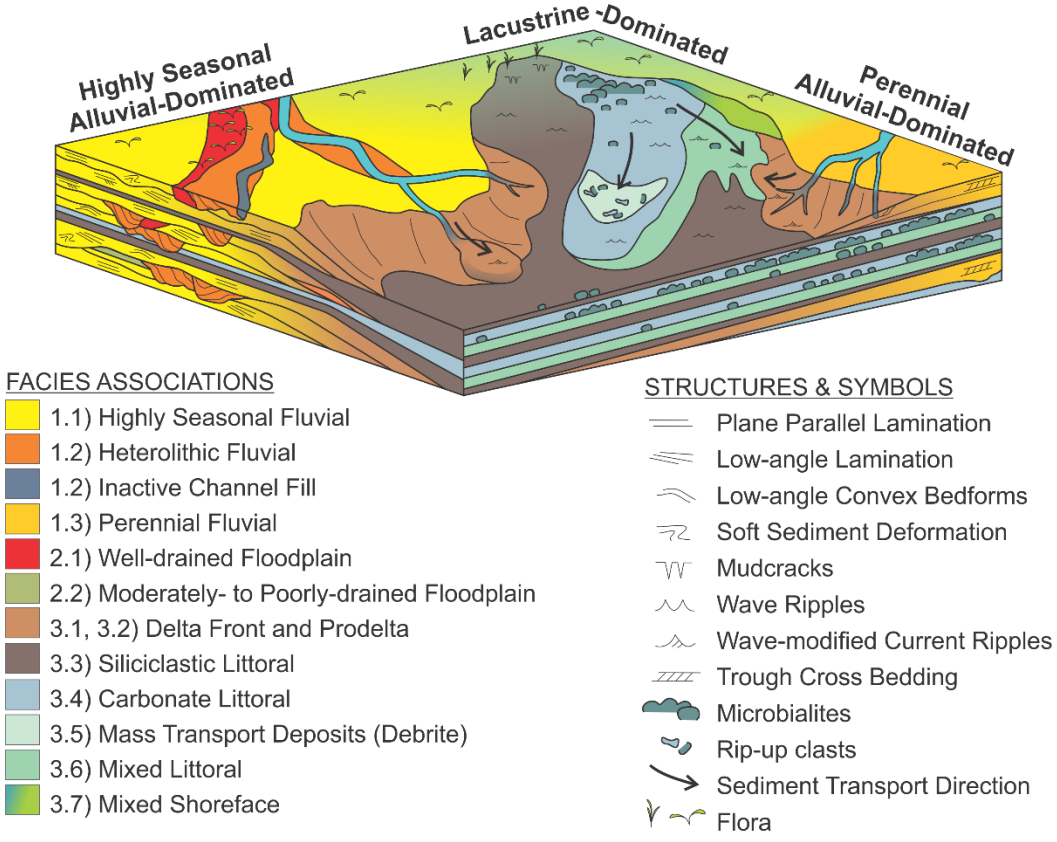

Figure 7. Box model of depositional environments. The diagram includes the three main depositional environments observed in Douglas Creek and Parachute Creek Member deposits: highly seasonal fluvial-dominated, littoral lacustrine-dominated, and perennial fluvial-dominated.

Figure 8. Highly seasonal fluvial deposits. A) Low-angle convex bedform. B) Plane parallel (PPL) laminations separated by an erosive amalgamation surface. C) Climbing ripples, capped by a sandy gray mudstone drape (F1). D) Mud intraclasts and mud rip-up lag deposit near scour surface. Also displayed is the horizontal transition between low-angle and plane parallel lamination. E) Low-angle lamination (LAL) cut by isolated trough cross stratification at the base of a channel, capped by low-angle and plane parallel lamination. F) Downstream accreting macroforms, a common characteristic of FA1.1.

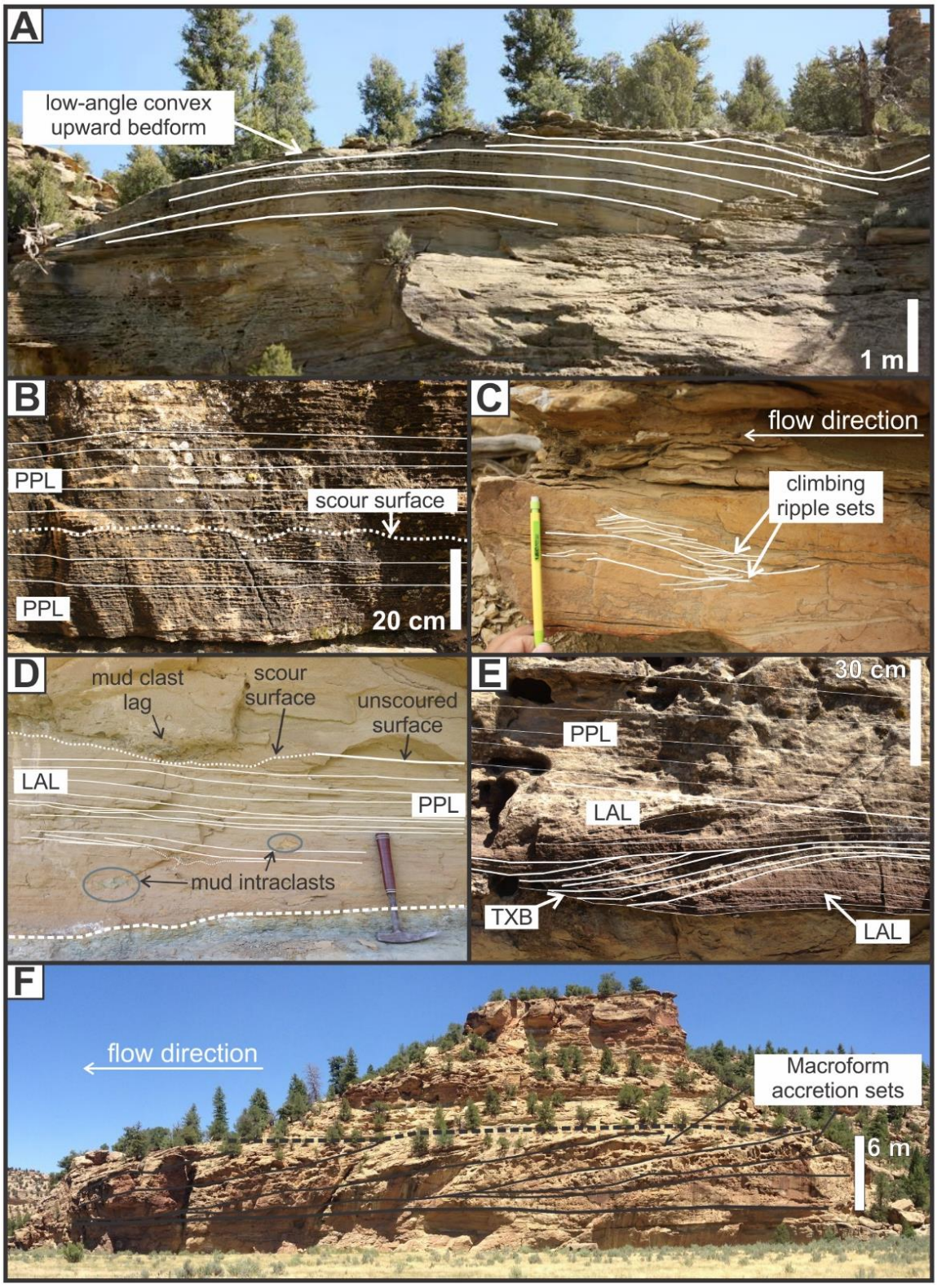
A
low-angle convex upward bedform
1 m
B
PPL
scour surface
PPL
20 cm
C
flow direction
climbing ripple sets
D
mud clast lag
scour surface
unscoured surface
LAL
PPL
mud intraclasts
E
30 cm
PPL
LAL
TXB
LAL
F
flow direction
Macroform accretion sets
6 m

Figure 9. Stacking patterns of the highly seasonal archetype. Outcrop image of highly seasonal fluvial deposits (FA1.1), heterolithic channels (FA1.2), and floodplain deposits (FA2.1) of Interval 1. A) Example from TB section. Note significant scale change from SW to NE. B) Interpretation of (A), with bodies numbered in order of deposition. The interpretation exemplifies the complex stacking and amalgamation of all facies. The thick sequences (>3 m, e.g., event #4) of UFR-dominated sandstone accumulate rapidly in downstream accreting macroforms under Froude supercritical flow conditions, which are commonly cut by heterolithic channels (e.g., event #5) interpreted as subsequent erosive conditions during waning flood stages or as perennial channels. Flow direction of UFR-dominated sandstone bodies is obliquely to the right into the image. C) Outcrop image of lower Interval 1 fluvial deposits from near JP section. D) Interpretation of (C). Another example of thick accumulations UFR-dominated sandstone cut or capped by heterolithic channels. The heterolithic channel represented by event #3 contains rhizoliths and is pedogenically modified, indicating that enough time passed for flora to become established on the filled channel before capped by subsequent deposits (event #4). Note visible accretion sets in event #2, and prominent low-angle convex-upward bedforms in event #7.

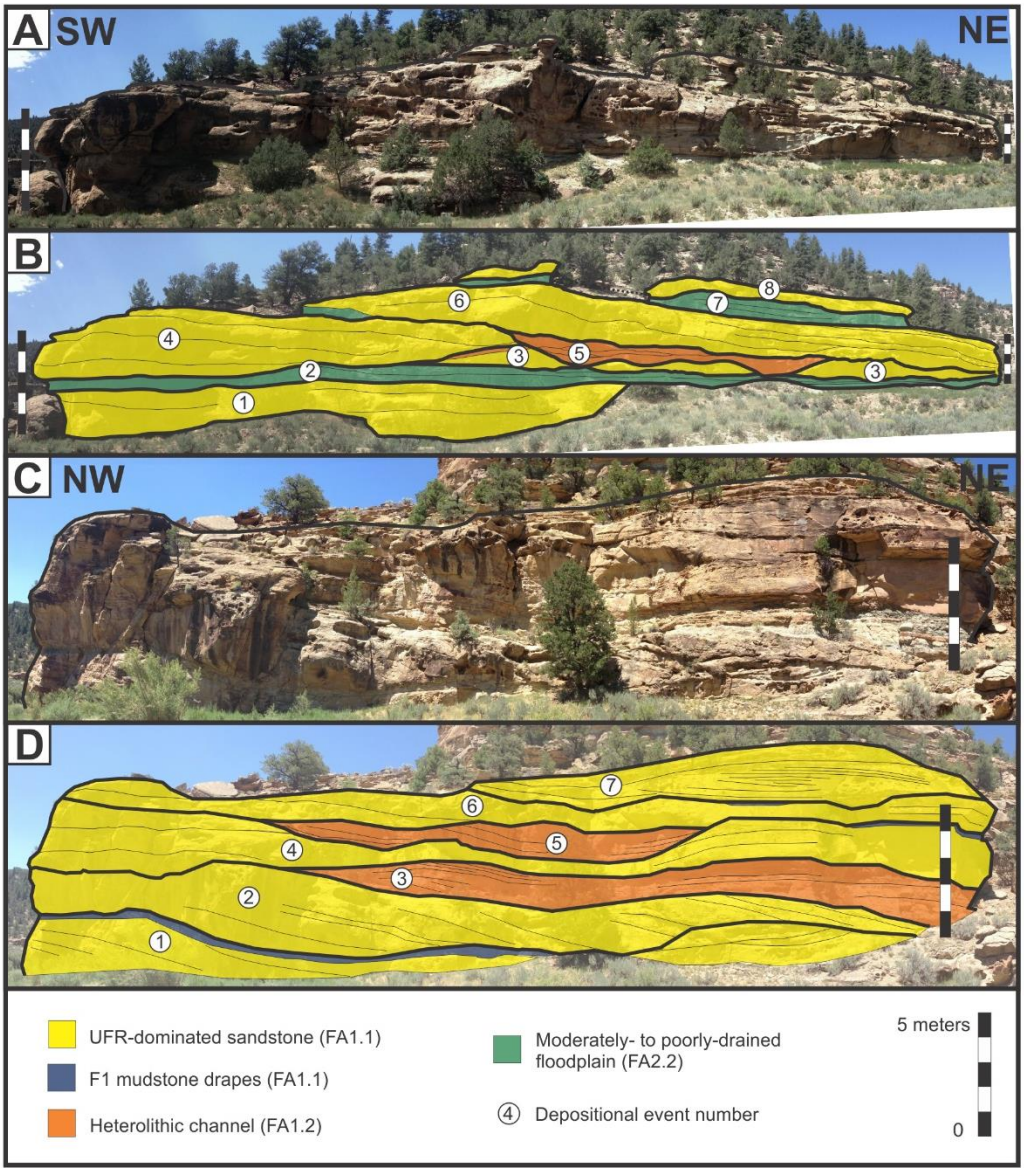
A SW
NE
B
1
2
3
4
5
6
7
8
3
C NW
NE
D
1
2
3
4
5
6
7
UFR-dominated sandstone (FA1.1)
F1 mudstone drapes (FA1.1)
Heterolithic channel (FA1.2)
Moderately- to poorly-drained floodplain (FA2.2)
④ Depositional event number
5 meters
0

iron concretions are common near the tops of beds. Mudstone intraclasts up to 10 cm, organic material, and rare bone fragments are found throughout beds.

FA1.1 bodies display a high degree of amalgamation both vertically and laterally. Tabular to lenticular beds have flat to undulating bases that exhibit 0.1-5 m of erosive downcutting. FA1.1 bodies contain up to eight vertically amalgamated beds that vary in thickness from 0.1 to 4 m. Coarse-grained lag deposits consisting of mud clasts, carbonate grains, and sandstone rip-up clasts are commonly present at the base of beds, but are most common and thickest (up to 0.5 m) in basal-most beds of amalgamated successions. The upper boundary of the uppermost bed is typically flat to slightly undulatory. Laterally-discontinuous layers of gray mudstone (F1) up to 0.2 m thick are found between some S1 bodies (Figure 9). Accretion sets are relatively common in FA1.1 and extend over 50 m laterally, and vertically extend up to 6 m from base to top.

FA1.1 channel elements are 40-1265 m (avg.=444 m) wide and 3-13.5 m (avg.=9 m) thick where measurable perpendicular to paleoflow (Figure 10). Paleoflow indicators suggest dominantly northward directed flow (ripple avg.=052, trough cross bed avg.=352; Figure 10). Macroform accretion sets indicate northeastern accretion (avg.=044; Figure 10). Where observed directly together, trough cross strata and accretion set data indicate similar paleoflow directions, suggesting accretion sets represent downstream-migrating barforms.

FA1.1 is characterized by thick accumulations of UFR structures, complex internal heterogeneity, downstream accreting macroforms, and a high degree of vertical and lateral amalgamation that can be interpreted as weakly-channelized highly seasonal UFR-dominated fluvial flood deposits from a semi-arid to sub-humid climate (Fielding et

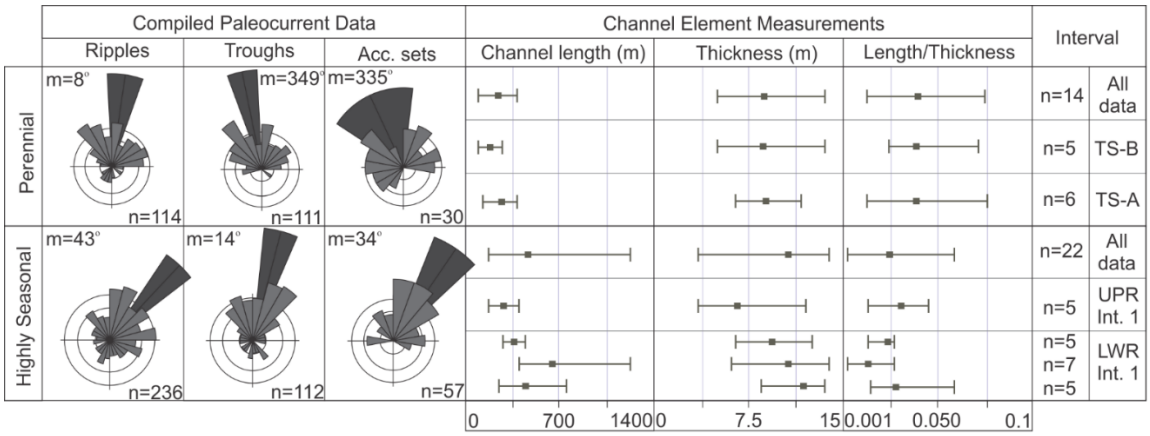

Figure 10. Compiled paleocurrent and measurements of fluvial bodies. Paleocurrent data are compiled from all measured sections. Channel element measurements are compiled and split by stratigraphic interval. Highly seasonal fluvial deposits of the Lower Interval 1 are further split according to stratigraphic height within the interval to show the waxing and waning of fluvial channel element size.

al. 2009, 2011; Plink-Bjorkland, 2015). S1 is interpreted as the result of mass sediment transport and rapid deposition during seasonal flooding, and the preservation of UFR structures indicates rapid changes from Froude supercritical to Froude subcritical flow velocities (Alexander et al., 2001; Fielding et al., 2009). The presence of low-angle convex-upward bedforms (antidunes) and climbing ripples indicates high sediment loads and deposition rates that exceed bedform migration (Allen, 1984), and the presence of convolute bedding and flame structures further suggest rapid deposition trapping significant water content and subsequent dewatering (Mills, 1983). The complex internal arrangement of UFR structures indicates rapidly changing flow conditions locally within the channel, interpreted as a result of redistribution of flow as sediment is rapidly deposited. Trough cross strata are interpreted to represent Froude subcritical flow conditions during early or waning stages of seasonal floods, or when observed within UFR strata, a result of pulsed flooding or local shielding from high velocity flow by macroforms (e.g., Fielding et al., 2009). Laterally-discontinuous mudstone (F1) is interpreted as waning and low-stage flow deposits, in which clay and silt draped flood-stage sand deposits (Fielding et al., 2009).

FA1.2: Heterolithic Fluvial Bodies

FA1.2 consists of heterolithic interbedded current rippled sandstone (S4), gray mudstone (F1), green-gray siltstone (F2), and red-tan siltstone (F3) in lenticular morphologies (Figures 9, 11A). Individual beds vary from 0.01-0.3 m thick, have sharp to gradational vertical contacts, and commonly grade laterally, resulting in highly heterolithic packages. Beds parallel the lenticular packages in which they are contained,

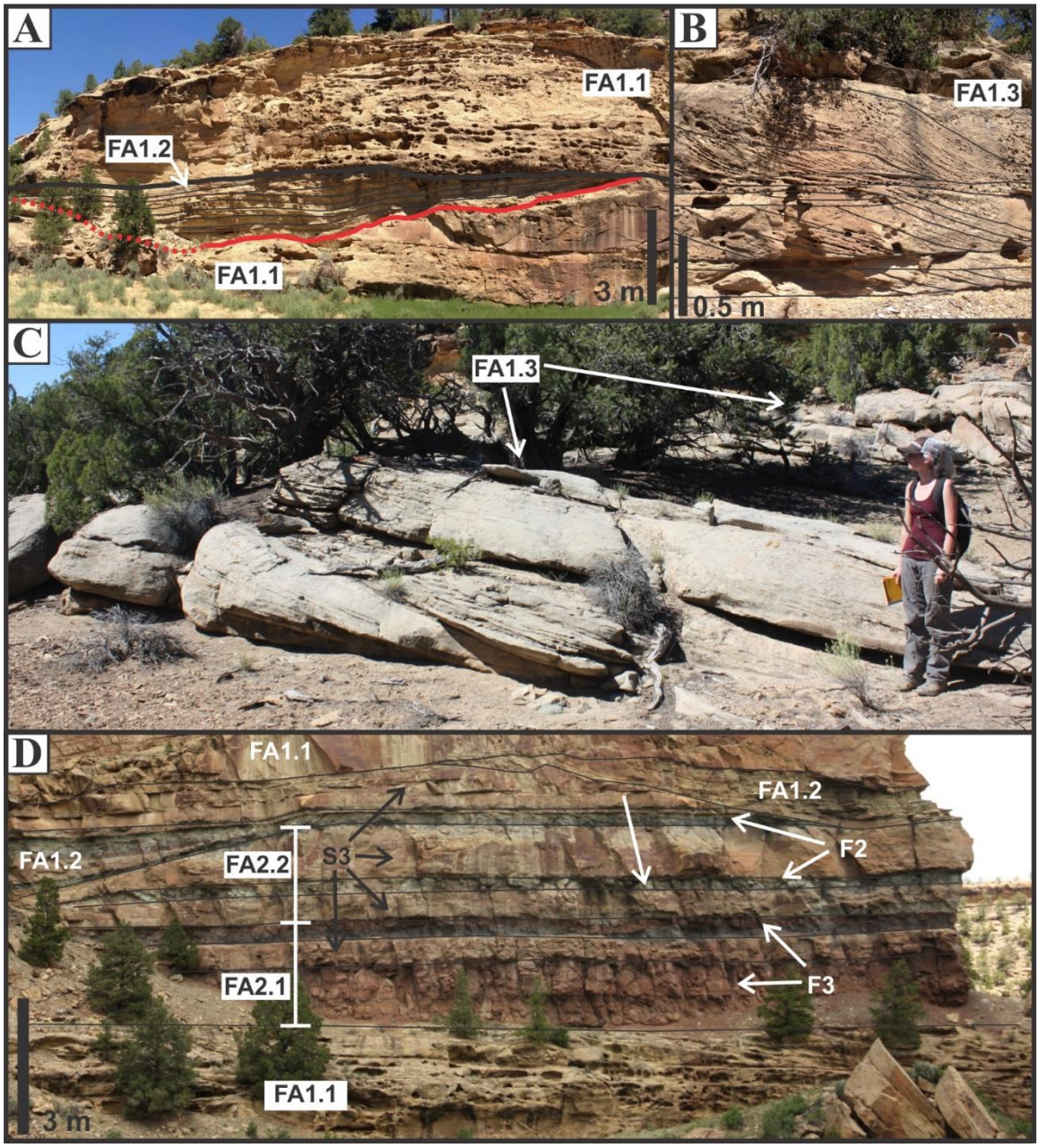

Figure 11. Fluvial and floodplain deposits. A) A heterolithic channel (FA1.2) cuts into UFR-dominated fluvial sandstone (FA1.1). B) Trough cross stratification characteristic of perennial fluvial deposits (FA1.3). C) Typical exposure of perennial fluvial deposits (FA3.1) interbedded with poorly-exposed fine-grained deposits. D) A floodplain succession (FA2.1 and FA2.2) that overlies UFR-dominated fluvial sandstone (FA1.1) and is overlain by FA1.1 and heterolithic fluvial channels (FA1.2). Note the vertical transition from FA2.1 to FA2.2, indicating a rising water table.

where beds become thinner, finer-grained, and inclined at package margins. Thick accumulations of gray mudstone (F1) commonly cap interbedded heterolithic deposits. Most FA1.2 stories erode into UFR-dominated fluvial bodies (FA1.1) and relatively few into floodplain deposits (FA2.1, 2.2). FA1.2 stories are 8-350 m wide and 2-9 m thick. Limited paleoflow indicators from ripples and accretion sets span all directions, though are most dominantly north-northeast.

FA1.2 is interpreted as fluvial deposition in low-velocity, narrow and shallow streams present during waning monsoonal flood conditions or during the dry season in a highly seasonal climate regime. The heterolithic deposits represent variable flow velocity, where sandstone represents deposition during relatively higher flow velocity and mudstone indicates low velocity deposition or suspension settling (Miall, 2013). The presence of colored fine-grained deposits (F2 and F3) is interpreted to be the result of pedogenic modification subsequent to deposition. Thick accumulations of gray mudstone (F1) in FA1.2 is interpreted as inactive channel fill (Miall, 2013). Accretion direction and current ripple paleocurrent data are rarely found together in FA1.2; in two cases, current ripples are ~60-90° offset from accretion direction, suggesting oblique to lateral migration of channel macroforms.

Alternatively, FA1.2 may represent active perennial fluvial erosion and deposition that is not linked to and occurs on a separate timescale than that of FA1.1, such as erosively-based channels that are linked to a rise in base level observed in the Sunnyside Delta Interval of Nine Mile Canyon, Uinta Basin (Keighley et al., 2003). However, this interpretation is not preferred as FA1.2 is most commonly contained within amalgamated bodies of FA1.1, suggesting the two facies associations are intimately linked.

FA1.3: Trough Cross Bed-Dominated Fluvial Bodies

FA1.3 is composed of trough cross bed-dominated sandstone (S2) in erosive lenticular bodies (Figures 11B-C). S2 contains very fine to medium sand with prevalent trough cross stratification (60-100%) with subordinate current ripples, climbing ripples, plane parallel lamination, and convolute bedding. Trough cross sets are 0.1-0.5 m thick. Coarse sand and carbonate grains commonly occur in lag deposits. Significant tar accumulation is also present in S2 bodies, which results in a deep gray-purple color in outcrop.

FA1.3 exhibits downcutting up to 10 m into poorly-exposed fine-grained facies; where erosive contacts are exposed, FA3.1 cuts into lacustrine facies associations (FA3.3, 3.4, and 3.5) or into floodplain deposits (FA2.1, 2.2). FA1.3 bodies are amalgamated vertically and laterally, and are 140-400 m wide (avg.=200 m) and 4-13 m thick (avg.=6.6 m). Paleoflow spans W-N-E directions, as informed by troughs (avg.=352), ripples (avg.=006), and flute casts (avg.=004; Figures 5, 10). Macroform migration occurs dominantly in W-SW or NE directions (avg.=341), suggesting oblique to downstream migrating macroforms (Figure 10).

FA3.1 is interpreted as perennial fluvial deposits, characterized by relatively continuous erosion, deposition, and macroform migration (Cant and Walker, 1976; Miall, 1978, 2013; Bridge, 1993; Hickin, 1993; Galloway and Hobday, 1996; Horn et al., 2012). Paleoflow indicators suggest macroforms were dominantly obliquely- to downstream-accreting in W and NE directions from dominantly northward directed flow. Laterally adjacent lacustrine facies (FA3.3, 3.4, 3.5) indicate that FA3.1 was an erosive, marginal fluvial-lacustrine system.

FA2.1: Well-drained Floodplain

FA2.1 consists of 0.5-4 m thick packages of poorly-consolidated red-tan sandy siltstone (F3) and tabular beds of massive sandstone (S3) (Figure 11D). F3 can be mottled and commonly contains sparsely scattered rhizoliths (vertically up to 50 cm), calcite nodules, ferrous nodules, and 2-30 cm vertical burrows or branching burrow networks. Interbedded with F3 are 0.05-0.5 m thick, sharply-based, non-erosive, massive tabular sandstone beds (S3). S3 commonly fines upwards and also laterally. The lateral extent of FA2.1 is limited to several hundred meters as it is commonly cut by FA1.1 or is slope forming.

FA2.1 is interpreted as well-drained floodplain deposits. The presence of calcite nodules, ferruginous nodules, and well-developed red color of F3 suggests pedogenic modification in well-drained conditions expected in semi-arid to sub-humid climates where evapotranspiration is significantly greater than precipitation (Machette, 1985; Bown and Kraus, 1987; McCarthy and Plint, 1998; Kraus, 1999; Driese and Ober, 2005). Sparsely scattered rhizoliths and bioturbation further suggest limited biological influence attributable to semi-arid and sub-humid landscapes (Fielding et al., 2011). S3 is interpreted as overbank splay deposits intimately linked with FA1.1 or FA1.3 fluvial deposits, in which channels were breached and deposited sand across the floodplain (Bown and Kraus, 1987; Donselaar et al., 2013).

FA2.2 Moderately- to Poorly-drained Floodplain

FA2.2 consists of slightly calcareous, blocky-weathering green-gray siltstone with variable sand content (F2) interbedded with 0.02-1.0 m thick beds of tabular massive

sandstone (S3) (Figure 11D). F2 beds commonly exhibit vertical gradational color changes and light mottling, and some exposures are indurated with surficial clay weathering. Calcite nodules and 2-10 cm burrows are present but rare. Rhizoliths are common in F2, but are sparse and limited to 15-20 cm vertical extents. FA1.4 packages commonly coarsen upwards with thickest S3 beds at the top of successions.

FA1.4 is interpreted as a moderately-drained to poorly-drained floodplain. Green-gray colored siltstones indicate high water table levels and reducing conditions (Myrow, 1990), and gray colored siltstone is interpreted as water logged gleysols (Kraus, 1999; Driese and Ober, 2005). Indurated beds are interpreted as groundwater calcretes formed by groundwater interactions that form calcite cement (Alonso-Zarza, 2003). As in FA2.1, S3 is interpreted as overbank fluvial deposits (Bown and Kraus, 1987).

FA3.1 Delta Front

FA3.1 consists of interbedded gray mudstone (F1), current rippled sandstone (S4), and wave rippled sandstone (S5) that occurs in laterally-continuous to lenticular coarsening-upwards packages up to 4 m thick (Figure 12A). Contacts between 0.01-0.1 m thick beds are sharp or gradational. Packages are slightly calcareous and contain scattered ostracod carapaces, fish scales, and *Skolithos*. The base of the successions commonly exhibit 0.01-0.05 m thick beds of F1 and S5 that are normally or reverse graded, lenticular to tabular, horizontally bedded, and contain wave ripples. Current rippled sandstone (S4) also contains minor plane parallel lamination, low-angle lamination, climbing ripples, and trough cross beds. S4 is increasingly common and can be amalgamated as packages coarsen upward. Laterally-extensive 0.1-1.0 m thick beds of S4

Figure 12. Deltaic, siliciclastic littoral, and carbonate littoral deposits. A) Coarsening upwards package of delta front facies association (FA3.1), with wave rippled sandstone (S5) and current rippled sandstone (S3) interbedded with gray mudstone (F1). B) Sandy delta front cut by a mudstone-filled distributary channel (FA3.1), capped by a prodelta deposits (FA3.2) consisting of gray mudstone (F1) between turbidite sandstone beds (S4). A mixed shoreface (FA3.7; Fig. A3-2H) caps the deltaic deposits. C) A thick package of clastic littoral deposits (FA3.3) consisting of interbedded wave rippled sandstone (S5) and green-gray mudstone (F2). D) Close up of FA3.3, including mudcracks in gray mudstone (F1), and wave ripples (WR) in sandstone (S5). E) Grainstone (C2) of carbonate littoral facies association (FA3.4). F) Thin section of ooilitic packstone (C2), showing ostracods at the center of some ooid grains. G) Brown microbialites of the Upper Microbialite Marker Bed (FA3.4), a locally correlatable microbialite marker in Main Canyon. H) Carbonate mudstone facies (C1) capped by microbialite packages (C3) of FA3.4, making up the C-Marker

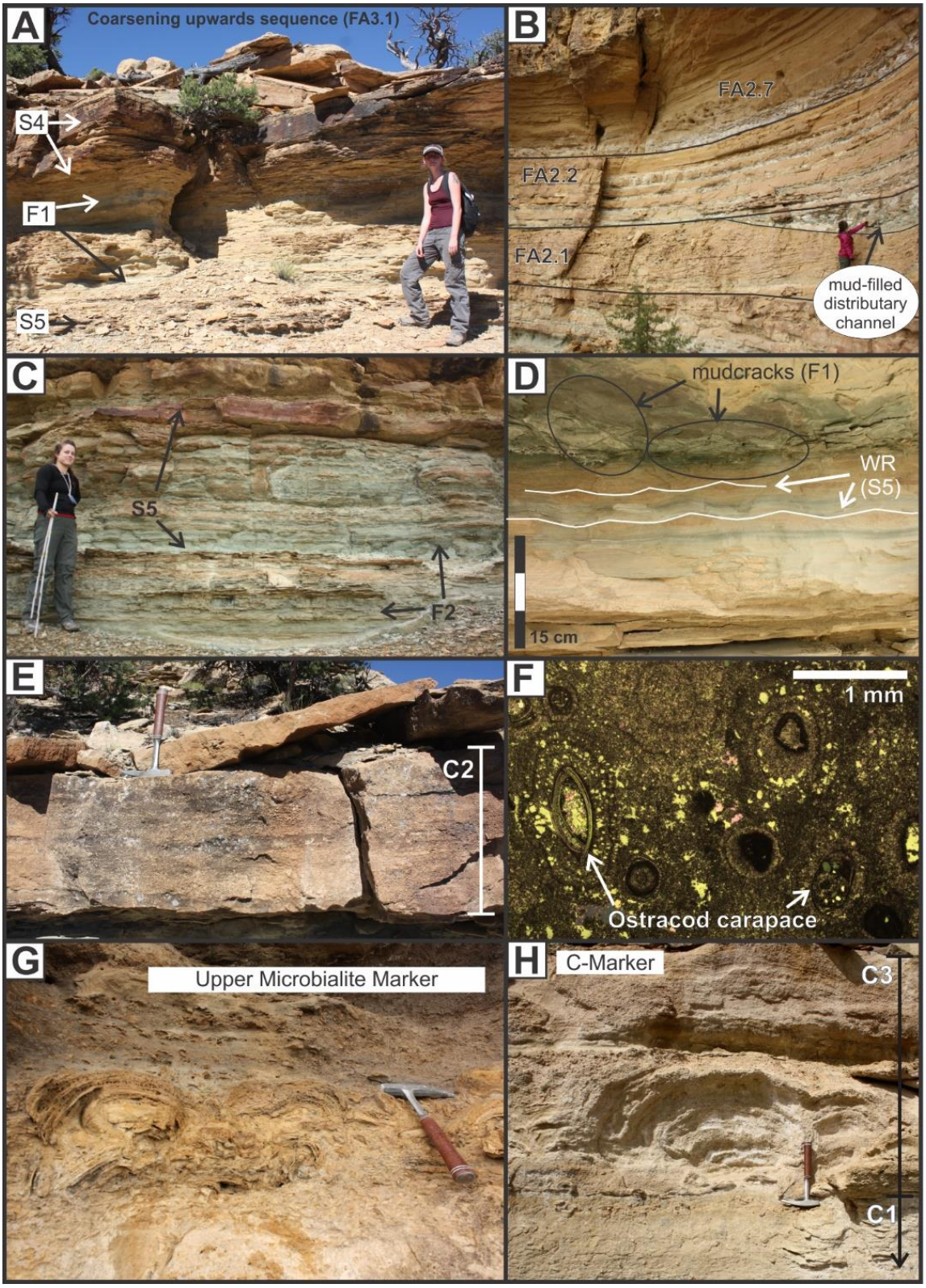
A
Coarsening upwards sequence (FA3.1)
S4
F1
S5
B
FA2.7
FA2.2
FA2.1
mud-filled distributary channel
C
S5
F2
D
mudcracks (F1)
WR (S5)
15 cm
E
C2
F
1 mm
Ostracod carapace
G
Upper Microbialite Marker
H
C-Marker
C3
C1

cap thinly interbedded F1-S5-S4 packages. Current ripple and flute casts indicate a strong northward sediment transport direction (Figure 5). FA3.1 occurs as laterally-extensive packages interbedded with FA1.1, 1.3, 3.3, or 3.5, or FA3.1 within lenticular bodies cuts into underlying facies up to 4 m.

FA3.1 is interpreted as delta front deposits. Coarsening upwards sequences indicate basinward fluvial-deltaic progradation. The occurrence of wave ripples and wave-modified current ripples at the base of successions suggest oscillatory current reworking of sediment. The dominance of current ripples and at the top of successions suggests increased fluvial input during basinward progradation, and paleocurrent data are consistent with fluvial paleocurrent measurements. Erosively-based, lenticular morphologies of some FA3.1 deposits are interpreted as distributary channels that are linked to distal mouthbar deposits, in which channels are eroded and subsequently filled during the progradation of deltaic-mouthbar complexes (Schomacker et al., 2010; Rosenberg et al., 2015). Apparent tabular morphologies are associated with widespread deltaic progradation.

FA3.2 Prodelta

FA3.2 consists of alternating beds of laterally-continuous of gray mudstone (F1) and massive tabular sandstone (S3) (Figure 12B). Individual beds are tabular, 0.05-0.5 m thick, and have sharp contacts. S3 beds are very fine-grained sandstone, fine-upwards, and are massive. F1 may coarsen- or fine-upwards. Both facies exhibit fish scales, *Skolithos,* and are calcareous. FA3.2 packages are 2-5 m thick, and exhibit overall coarsening upward and bed-thickening upward trends.

FA3.2 is interpreted to have been deposited in a prodelta environment. Laterally-extensive, tabular beds indicate deposition over a broad area, and the coarsening upward successions suggest overall deltaic progradation. Deposition of S3 was likely driven by episodic sand input from a fluvial source that resulted in tabular, non-erosive sandstone beds, and the bed scale fining upwards pattern is consistent with hyperpycnal flows that enter the lake from an updip fluvial source and flow along the lake bed (Bhattacharya and MacEachern, 2009). Gray mudstone (F1) is interpreted to represent low-velocity deposition or suspension settling during intermittent quiescence (Olariu and Bhattacharya, 2006).

FA3.3 Clastic Littoral

FA3.3 consists of gray mudstone (F1) and gray-green siltstone (F2) interbedded with wave rippled sandstone (S5) and current rippled sandstone (S4) (Figures 12C-D). F1 and F2 are massive with mudcracks or wave ripples. Tabular beds of 0.02-0.1 m thick wave (S5) or current rippled (S4) sandstone exhibit flat, non-erosional contacts with F1 and F2. In some instances, S4 occurs as intermittently in layers that are convoluted within fine-grained facies. Isolated ostracod carapaces, *Skolithos*, and fish scales occur throughout FA3.3. FA3.3 packages are 0.1-5 m thick and are laterally-continuous except where cut by fluvial or deltaic facies.

FA3.3 is interpreted as a siliciclastic-dominated littoral lacustrine environment, characterized by suspension deposition and reworking of fine-grained clastic input from fluvial sources in relatively low-energy, shallow environments. F2 is interpreted to be slightly reduced fine-grained deposits (Myrow, 1990). Sand is interpreted to be reworked

via osciallatory currents (S5) or in clastic shoals (S4). Intermittent convoluted lenticular sandstone beds are interpreted as the result of compaction-associated dewatering of mudstone layers during burial (Burst, 1976; Mills, 1983). The heterolithic nature of FA2.3 indicates mixed depositional energies expected in shallow lacustrine settings, where fine grains settled during quiescent periods between relatively higher energy environments associated with wave or current reworking of sand.

FA3.4 Carbonate Littoral

FA3.4 consists of carbonate mudstone (C1), grainstone (C2), and microbialite (C3) facies (Figures 12E-H). C1 occurs as 0.02-2 m thick, laterally-continuous, organic-poor carbonate mudstone and wackestone beds that contain sparse ooid grains and ostracod carapaces. C2 is 0.05-1 m thick, laterally-continuous ostracodal and ooilitic packstones or grainstones with a carbonate mud matrix or with spar cement, respectively. C1 and C2 commonly grade into each other, or beds are separated by a non-erosive contact. Thin section analysis indicates ooids are the most abundant grains in C1 and C2, although ostracods are common and form the nucleus of some coated grains (Figure 12F). Sedimentary structures are generally absent in C1 and C2. C3 is characterized by fabrics associated with microbialites, including laminated mats, stromatolitic mounds and columns, and thrombolitic textures. Isolated stromatolite heads are up to 0.5 m tall, and laterally-continuous, connected stromatolite mound beds are up to 1 m thick. Ostracods and ooid grains are common within microbialite fabrics.

FA3.4 is interpreted as a carbonate-dominated littoral to sublittoral lacustrine environment. The coated grains and lack of carbonate mud in C2 indicates a higher

energy, wave-influenced environment, such as a lacustrine bar, shoal, or shoreline where most mud was winnowed out (Milroy and Wright, 2002; McGlue et al., 2010). The presence of large microbialites (C3) suggests deposition within the photic zone and represents a mixture of depositional energy (Frantz et al., 2014; Awramik and Buchheim, 2015). The presence of carbonate mudstone and wackestone (C1) indicates more quiescent environments where carbonate mud precipitated in the water column and settled on the lake bottom.

FA3.5 Mass Transport Deposits

FA3.5 consists of thick, laterally-extensive accumulations of clast-rich carbonate (C4), which is composed of a wackestone to ooilitic packstone matrix with abundant subangular-subrounded ooilitic packstone rip-up clasts (Figures 13A-B). Rip up clasts are 1-5 cm wide, 0.25-2 cm thick, and are slightly imbricated, indicating a E-NE paleoflow (Figure 5). Weakly to non-erosive C4 beds are 0.1 to 2.5 m thick and are stacked in amalgamated successions up to 4 m thick. Beds display slight normal grading, whereas overall packages coarsen upwards with less carbonate mud and more ooid grains in the matrix.

FA3.5 is interpreted as subaqueous mass transport deposits. Thick beds with poorly-sorted rip-up clasts within carbonate matrices and imbrication indicates mass movement E-NE into the basin. Carbonate material was likely sourced from nearshore carbonate factories, and mass movement is likely associated with large storms or potentially induced by seismic activity (Toro and Pratt, 2015).

Figure 13. Debrite and mixed clastic-carbonate lacustrine deposits. A) Mass transport carbonate deposits (C4) of FA3.5. This thick, stacked succession represents the Mass Transport Marker Bed. Inset box highlights location of (B). B) Detailed image of ooilitic packstone rip-up clasts in oolitic packstone (C4). C) Mixed clastic-carbonate deposition of FA3.5, with calcareous gray mudstone (F1), highly rippled sandstone (S3) interpreted as a clastic shoal, and a microbialite mat (C3). D) An isolated microbialite mound (C3) within calcareous gay mudstone (F1) (FA3.5). E) Laminated mixed clastic-carbonate bed (M1, FA3.5). Individual laminae are separated by grain size interpreted as a result of traction currents. F) A bioturbated representation of M1, interpreted as nearshore, littoral mixed clastic-carbonate environment (FA3.5). G) Massive mixed clastic carbonate bed (M2) within green-gray mudstone (F2), interpreted as relatively high energy mix of clastic and carbonate grains (FA3.6). Carbonate intaclasts up to 5 cm are found in M2. H) A shoreface succession (FA3.7). Carbonate mudstone (C1) represents the lower shoreface, and grades into the massive mixed clastic-carbonate facies (M2) representing the high energy, upper shoreface.

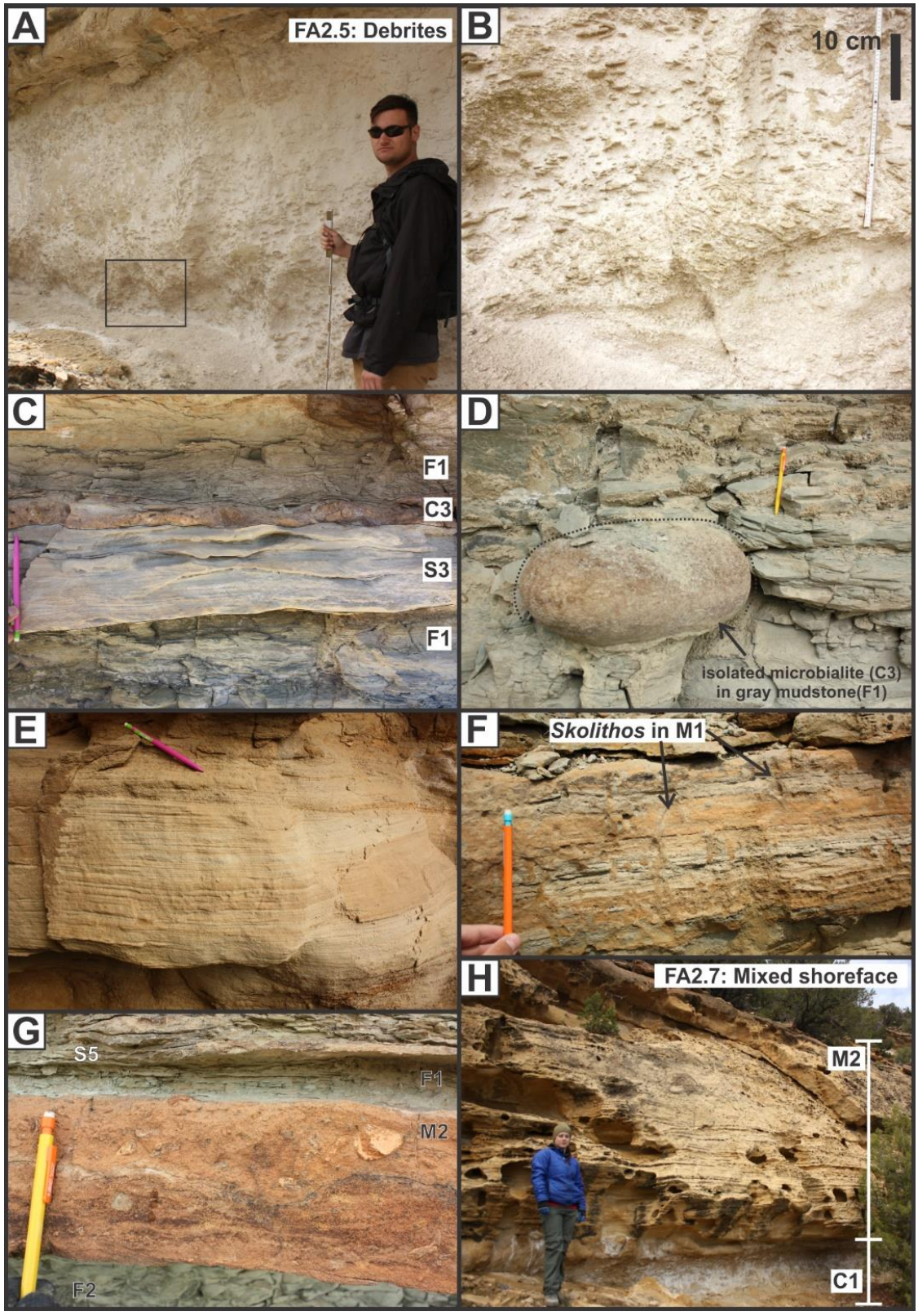
A
FA2.5: Debrites
B
10 cm
C
F1
C3
S3
F1
D
isolated microbialite (C3)
in gray mudstone(F1)
E
F
Skolithos in M1
G
S5
F1
M2
F2
H
FA2.7: Mixed shoreface
M2
C1

FA3.6 Mixed Clastic-Carbonate Littoral

FA3.6 consists of high-frequency alteration of siliciclastic facies (FA3.1 and 3.3) with carbonate facies (FA3.4) and mixed carbonate-siliciclastic facies (M1 and M2) (Figure 13C-G). M1 occurs as tabular, laminated beds composed of very fine to fine sand with similarly sized ostracods and ooid grains; ratios of clastic and carbonate sediment vary on the lamina and bed scale. M1 beds are dominated by wavy and low-angle lamination and commonly exhibits heavy *Skolithos* bioturbation. M2 occurs as tabular, massive beds of mixed very fine to medium sand with ostracods, fish scales, ooid, and peloid grains up to 4 cm. Trough cross strata is locally observed in M2. Individual beds in FA3.6 are generally 0.05-0.15 m thick, but can be as thick as 0.5 m. Packages of FA3.6 are up to 6 m thick. Current ripple paleocurrent data compiled from FA3.6 span all directions but on average are SE directed (avg.=127; Figure 5). Wave ripples indicate oscillatory currents directed NE-SW (Figure 5).

High-frequency interbedded FA3.3 and FA3.4 are included as a separated FA3.6 to highlight the distinct nature of temporally mixed siliciclastic and carbonate beds (Mount, 1984; Tucker 2003). As FA3.6 commonly caps thick siliciclastic accumulations (FA3.1, 3.2, 3.3), it is interpreted to represent the gradual ‘turning off’ of local fluvial input and transition into a carbonate-dominated environment. The occurrence of spatially mixed siliciclastic and carbonate texture beds (M1 and M2) is interpreted as sporadic storm mixing that can transfer and mix sediment across depositional environment boundaries, or occurs in transitional areas of siliciclastic and carbonate depositional environments (Mount, 1984; McNeill et al., 2004; Quesne et al., 2009). The variable paleocurrent data indicate sediment mixing across depositional systems, where fluvial

input was directed N-NE (as indicated by FA3.1) and subsequently reworked parallel to shore on average to the SE.

FA3.7 Mixed Shoreface

FA3.7 consists of carbonate mudstone (C1) and thick accumulations of massive mixed clastic-carbonate deposits with minor trough cross strata (M2). The base of FA3.7 contains 0.1-1 m thick beds of laterally-continuous C1, that is capped by accumulations up to 5 m thick of laterally-continuous M2 (Figure 13H). The transition between C1 and M2 is gradational, sharp, or a 0.1-0.3 m zone of thinly interbedded C1 and M2.

FA3.7 is interpreted as a lacustrine shoreface succession. C1 is interpreted to represent a quiescent lower shoreface to sublittoral environment characterized by suspension settling of carbonate mud. Thick accumulations of M2 is interpreted as a high energy shoreline characterized by winnowing of mud and reworking of lacustrine carbonate grains with clastic grains from a terrestrial source (Milroy and Wright, 2002; McGlue et al., 2010).

FLUVIAL FACIES MODELS

Two distinct fluvial morphologies dominate fluvial deposition in the Main Canyon study area: UFR-dominated fluvial deposits (FA1.1) and associated heterolithic channels (FA1.2) interpreted as a highly seasonal fluvial system, and trough cross bed-dominated fluvial deposits (FA1.3) interpreted as part of a perennial fluvial system (Figure 4). The different external and internal architecture of the two major fluvial bodies indicates different controls on fluvial sediment transport and deposition. As controls and facies models of perennial fluvial systems are well-established (Cant and Walker, 1976; Bromley, 1992; Bridge, 1993; Hickin, 1993; Horn et al., 2012; Miall, 2013) and highly seasonal fluvial models are discussed only in recent literature (Fielding et al., 2009, 2011; Plink-Björklund, 2015), the ensuing discussion is focused using Main Canyon highly seasonal fluvial deposits to expand current highly seasonal fluvial facies models.

Macroforms are notably poorly-developed in modern highly seasonal rivers, and the exact processes of sediment deposition and barform migration in extended flood-induced UFR conditions remains enigmatic (Langford and Bracken, 1987; Ashworth, 1996; Alexander et al., 1999; Uba et al., 2005; Fielding, 2006; Alexander, 2008; Fielding et al., 2009; Nicholas et al., 2016). Limited macroform development has been interpreted as a result of high deposition rates and extended variable Froude supercritical flow conditions, or that observation of developed macroforms is potentially limited by lateral extent and directional cut of exposures in both modern and ancient examples (Fielding et

al., 2009, 2011; Plink-Björklund, 2015). However, the highly seasonal fluvial deposits in Main Canyon exhibit exceptionally well-developed, aggradational downstream-accreting macroforms that are up to 6 m thick (Figure 8F). The best outcrops are exposed parallel to paleoflow, where the very low-angle accretion sets formed by low-angle lamination are easily visible. The exceptional development of downstream accreting macroforms observed in Main Canyon is linked to sustained UFR conditions that allowed systematic aggradational accumulation of macroforms during flooding events, and excellent parallel-to-flow outcrops that provide quality exposures. We predict that systematic macroform accumulation is common in other highly seasonal systems, but is cryptic in nature due to the very low-angle of accumulation and need for a parallel to flow directional cut for optimal viewing.

Main Canyon highly seasonal fluvial deposits are also unique from other published ancient highly seasonal fluvial successions in that they preserve erosionally-based heterolithic channels (FA1.2) within sandstone channels of FA1.1 (Figures 8A, 9). The heterolithic channels are interpreted to represent active fluvial erosion and deposition during waning flood conditions and into the dry season. Dry season channels and associated downstream- to laterally-accreting barforms are present in modern highly seasonal fluvial systems (Singh and Bhardwaj, 1991; Shukla et al., 2001; Jain and Sinha, 2004; Fielding et al., 2009; Chakraborty and Ghosh, 2010; Plink-Björklund, 2015); however, the deposits are subject to subsequent remobilization from high-discharge events associated with seasonal storms (Fielding et al., 2009). The preservation of heterolithic channels in Main Canyon may be a result of infrequent flooding that spans numerous years, which would allow dry season channels to fill with sediment to bankfull

capacity and be subsequently overlain by flood deposits. Such inter-annual flood variability is observed in the Burdekin River, in which the bulk of alluvium is transported during 10-16 year return floods (Fielding et al., 2009).

Alternatively or complementary to infrequent high-magnitude flood return intervals, high avulsion rates of seasonal flood channels would allow dry season streams to fill to bankfull capacity as main flood channels are active elsewhere. Avulsion is notably more common than systematic and erosive channel migration in modern highly seasonal rivers, due to low channel stability from superelevated, aggradational flood-stage deposits (Mohrig et al., 2000; Jain and Sinha, 2004; Chakraborty et al., 2010; Donselaar et al., 2013; Hajek and Edmonds, 2014; Plink-Björklund, 2015). Further, channels commonly avulse back to previously occupied locations and create highly amalgamated and aggradational bodies in distributary fan settings (Kumar and Tandon, 1985; Kumar, 1993; Bryant et al., 1995; Mohrig et al., 2000; Kumar et al., 2003), a depositional setting that can explain the complex stacking of UFR-dominated and heterolithic channels observed in Main Canyon (Figure 9).

In contrast, FA1.3 displays abundant Froude subcritical flow sedimentary structures such as current ripples and trough cross stratification, and obliquely- to downstream-accreting macroforms. These characteristics are typical of temperate-humid perennial fluvial systems that experience a relatively constant mean monthly discharge and associated sediment transport, deposition, and macroform migration rates, such as the Platte, Mississippi, or Athabasca rivers of North America (Blodgett and Stanley, 1980; Smith, 1987; Kesel et al., 1992; Hickin, 1993; Skelly et al., 2003; Horn et al., 2012). Whereas perennial rivers also experience periodic flooding, the difference between mean

annual discharge and flood stage discharge is small when compared to highly seasonal fluvial systems (Plink-Björklund, 2015). Main Canyon perennial channels are much more narrow and exhibit greater height to width ratios (mean=0.036) than that of the highly seasonal fluvial deposits (mean=0.025) (Figure 10). Also markedly different from the highly aggradational highly seasonal channels is the erosive nature of lenticular perennial channels in Main Canyon, which cut up to 10 m into underlying fine-grained facies.

VERTICAL TRENDS

The 180 m vertical study area is divided into three stratigraphic intervals based on the dominant facies assemblage (Figures 6, 7, 14, 15): (1) Highly Seasonal Alluvial-Dominated Interval 1 covers the basal ~60 m; (2) Lacustrine-Dominated Interval 2 within in the middle ~65 m; and (3) Interbedded Perennial Alluvial and Lacustrine Interval 3 of the uppermost ~45 m.

Interval 1

Interval 1 is dominated by a highly seasonal alluvial archetype and also contains deltaic and lacustrine deposits. A prominent flooding surface identified by 0.5-7 m thick lacustrine deposits present across the transect further separates Interval 1 into two packages: (1) lower Interval 1, a 45 m thick package dominated by highly seasonal alluvial archetype, and (2) upper Interval 1, a 15-18 m thick package dominated by highly seasonal alluvial archetype in the northwestern field area, and by lacustrine deposits interbedded with relatively thin highly seasonal alluvial deposits in the southeastern field area (Figures 6, 14, 15). At least six additional laterally discontinuous flooding surfaces are present in Interval 1 (Figure 6), recognized by lacustrine deposits generally <1 m thick that are cut by highly seasonal channel belt elements with carbonate rip-up clasts at the base. These flooding surfaces are most prominent in the southeastern field area and are also observed in the northwestern field area (Figure 6).

Figure 14. AMP measured section gigapan. A) AMP section with measured section overlay. B) Annotated facies association interpretation of (A).

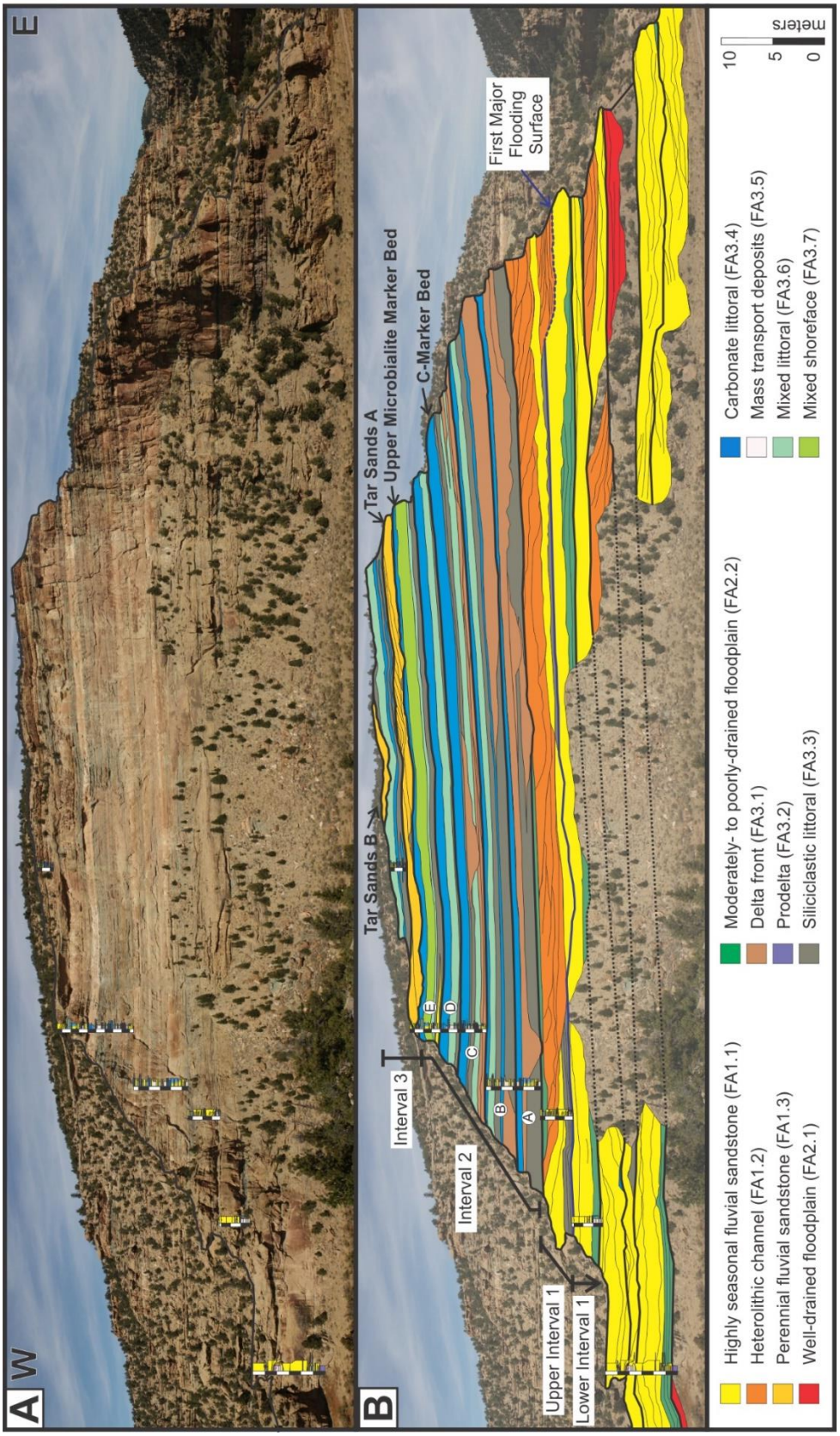
A
W
E
B
Tar Sands B
Tar Sands A
Upper Microbialite Marker Bed
C-Marker Bed
First Major Flooding Surface
Interval 3
Interval 2
Upper Interval 1
Lower Interval 1
A
B
C
D
E
Highly seasonal fluvial sandstone (FA1.1)
Heterolithic channel (FA1.2)
Perennial fluvial sandstone (FA1.3)
Well-drained floodplain (FA2.1)
Moderately- to poorly-drained floodplain (FA2.2)
Delta front (FA3.1)
Prodelta (FA3.2)
Siliciclastic littoral (FA3.3)
Carbonate littoral (FA3.4)
Mass transport deposits (FA3.5)
Mixed littoral (FA3.6)
Mixed shoreface (FA3.7)
meters
10
5
0

Figure 15. JP and PAR/PAB measured section gigapans. See Figure 14 for key. A) JP section. B) Interpretation of (A). C) PAR and PAB sections outcrop. D) Interpretation of (C). * and dashed line indicates largest measurable highly seasonal channel element (481 m) across PAR and PAB sections.

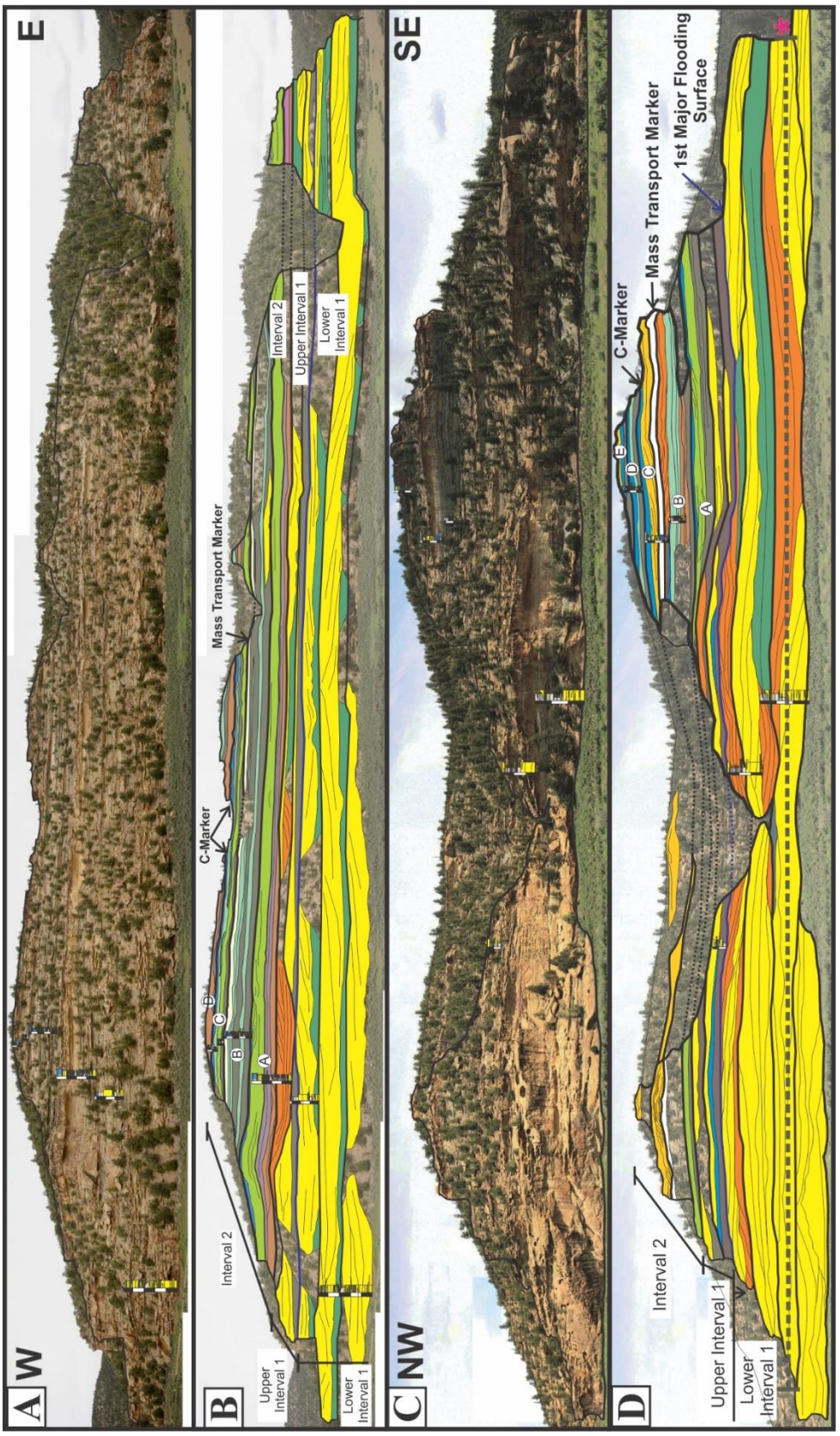
A W
E
B
Upper Interval 1
Lower Interval 1
Interval 2
C-Marker
Mass Transport Marker
Upper Interval 1
Lower Interval 1
A
B
C
D
C NW
SE
D
Interval 2
Upper Interval 1
Lower Interval 1
C-Marker
Mass Transport Marker
1st Major Flooding Surface
A
B
C
D
E

A distinct waxing and waning of channel element size is observed in Interval 1. Channels located in the stratigraphic middle of the lower Interval 1 are widest (avg.=676 m) and exhibit the smallest width:thickness ratio (avg.=0.015), whereas channels of upper Interval 1 are narrowest (avg.=222 m) with the largest width:thickness ratio (avg.=0.031) (Figure 10). Channel element dimensions are also variable across the transect: in the northwestern field area elements are thicker, wider, and more widespread, whereas in the southeastern field area elements are thinner and less laterally-extensive (Figure 6). Heterolithic channel stories become increasingly larger and more dominant from lower to upper Interval 1 (Figures 6, 14, 15).

Interbedded with and laterally adjacent to highly seasonal channel belt elements are 1-5 m thick floodplain elements. Well-drained, red paleosol floodplain deposits (FA1.3) are most common in the stratigraphically lowest part of lower Interval 1. Moderately- to poorly-drained floodplain deposits (FA1.4) become increasingly prevalent stratigraphically up and are the only floodplain deposits observed in upper Interval 1 (Figure 6).

Interval 1 records a period dominated by terrestrial deposition, representing an aggradational, floodplain-building fluvial system punctuated by relatively short intervals of lacustrine deposition. North-northeast directed paleoflow suggests that the main fluvial axis was likely located to the west-southwest. The observed stratigraphic changes in floodplain deposits, highly seasonal channel size, and increasing thickness of lacustrine deposits also indicate an overall rise in base level through Interval 1 (Figures 16A, B). Lake Uinta transgressions most likely occurred from E-NE to W-SW, as evidenced by

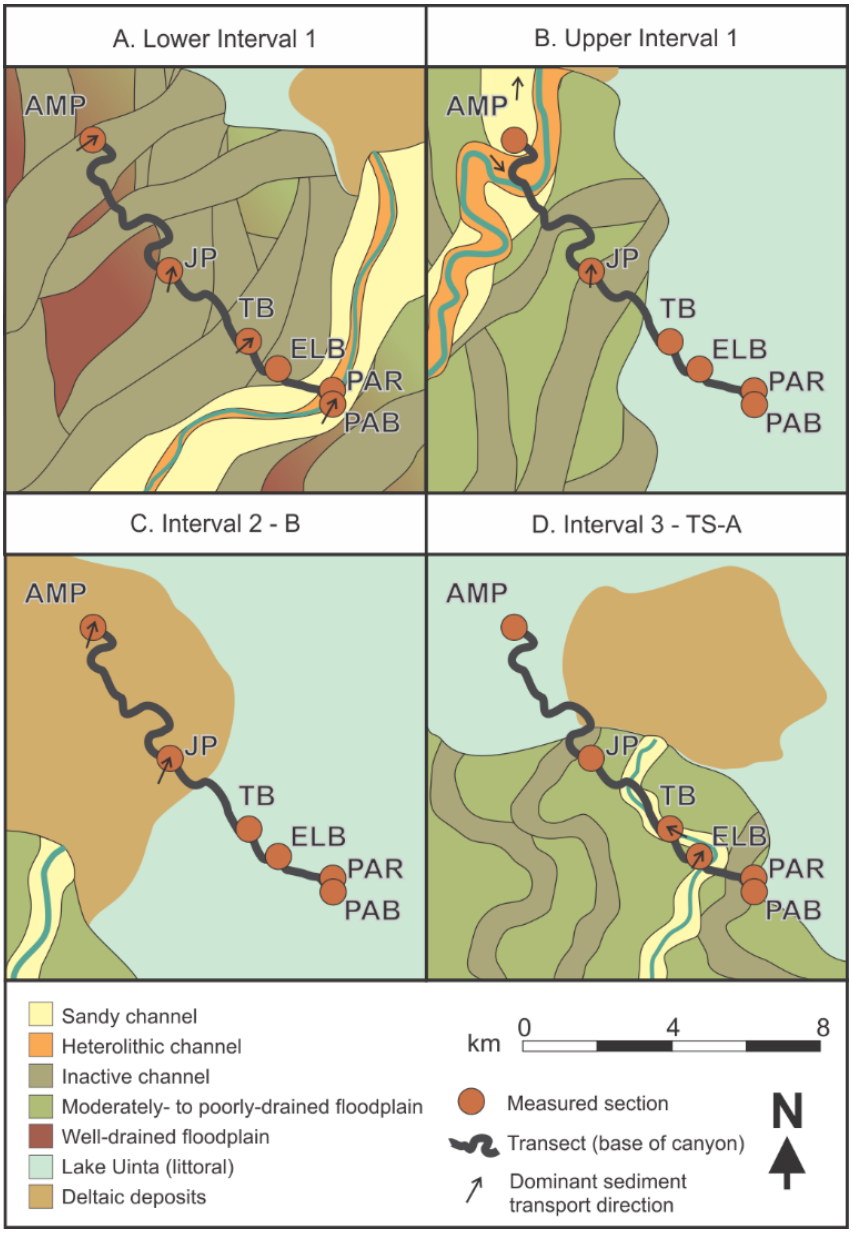

Figure 16. Paleogeographic reconstructions. See figure 6 for cross sectional interpretation.

paleocurrent data, thicker lacustrine deposits in the east, and larger channels in the west (Figure 6).

Interval 2

Interval 2 is a 65 m thick package of lacustrine deposits with isolated deltaic-mouthbar and fluvial elements. Interval 2 is divided into five 10-17 m thick laterally-continuous subintervals A through E that exhibit strong cyclicity between siliclcastic and carbonate deposition (Figures 5, 6). Subintervals are defined by a basal clastic unit (FA3.1, 3.2, 3.3), a middle mixed clastic-carbonate unit (FA3.6, 3.7), and an upper carbonate unit (FA3.4, 3.5). Siliciclastic packages generally exhibit slight coarsening upward trends. No strong coarsening or fining-upward trend is observable in mixed packages. Carbonate packages exhibit coarsening upward trends from carbonate mudstone and wackestone (C1) to packstone and grainstone (C2), or fining upward packages of packstone and grainstone (C3) capped by microbialites (C4).

Isolated channels are found in subintervals B, C, and D and are generally less than 50 m wide and 3 m thick. Channels are mud-filled, heterolithic interbedded sandstone and siltstone, or filled with massive amalgamated sandstone interpreted as mouthbar distributary channels (FA3.1; Schomacker et al., 2010). Thick, erosively-based trough cross bed-dominated (FA1.3) channels that are 100-200 m wide and exhibit up to 10 m of downcutting are present in subintervals C and E and are most prominent in the southeastern field area (Figures 6, 15). The channels are amalgamated with current ripples, trough cross stratification, convolute bedding, and are interpreted as perennial fluvial deposits (FA1.3) formed during short periods of terrestrial exposure.

Alternatively, these channels may represent distributary mouthbar channels that formed in a lacustrine environment (Schomacker et al., 2010).

The widespread cycling of siliciclastic, mixed siliciclastic-carbonate, and carbonate beds indicates broad, repeated changes in lacustrine depositional environments (Figures 5, 6, 16C). Paleocurrent data in siliciclastic deposits indicate strongly northward directed paleocurrents (Figure 5), signaling fluvial-deltaic input directed northward into Lake Uinta from terrestrial sources to the south. Paleocurrent data from temporally and spatially mixed clastic-carbonate packages (FA2.6) span all directions and dominantly to the southeast (Figure 5), which indicates that the fluvial system was intermittently active and that sediment mixing towards the SE was the dominant process. Wave ripples indicate a NW-SE trending shoreline (Figures 5, 16C). Carbonate accumulations that occur at the top of each subinterval indicate no local siliciclastic fluvial input into the basin and thick micritic microbialite accumulations suggest that carbonate material was locally sourced. Carbonate accumulations in subintervals C and E are thickest and most widespread (Figure 6), suggesting that these periods represent the most extended period of fluvial quiescence.

Interval 3

Interval 3 is characterized by perennial fluvial deposits (FA1.3) interbedded with poorly-exposed fine-grained floodplain (FA2.2), deltaic (FA3.2), and lacustrine (FA3.3, 3.4, 3.6) deposits. Two fluvial subintervals with significant tar accumulation are correlated to the Tar Sand Zone A and Tar Sand Zone B described by Blackett (1996) (Figures 5, 6, 14). Perennial fluvial channel belt elements within Tar Sand Zone A and

Zone B are 4-13 m (avg.= 6.5 m) thick, 150-400 m (avg.=210 m) wide (Figure 10), erode up to 10 m into underlying rock, and are vertically and laterally isolated within fine-grained facies. No significant difference in channel geometry is observed between the two fluvial zones (Figure 10).

Exposures of slope forming fine-grained deposits are limited, but where observed, moderately- to poorly-drained floodplain deposits (FA2.2) are generally less than 1-2 m thick. Delta front (FA3.1) deposits up to 3 m thick are present at the base and cap some fluvial channels within Tar Sand Zones A and B. Lacustrine deposits are laterally-extensive, organic poor, and up to 6 m thick. Siliciclastic (FA3.3), carbonate (FA3.4), and mixed clastic-carbonate (FA3.6) deposits are present; however, poor exposures limit characterization of lacustrine cyclicity in Interval 3.

Interbedded fluvial and lacustrine deposits indicate fluctuating relative lake levels and sediment delivery through at least two regressive-transgressive cycles following Interval 2. Flute casts in deltaic deposits indicate northward directed sediment transport into the basin. Paleocurrent data indicate west and northward directed fluvial sediment transport. The thick accumulations of interbedded lacustrine deposits and relatively thin, poorly- to moderately-drained floodplain (FA2.2) elements indicate the fluvial system was very close to the Lake Uinta shoreline and highlights the limited floodplain building nature of perennial channels in Main Canyon (Figure 16D).

DISCUSSION

The physical characteristics of sedimentary deposits are a result of sediment supply, grain size distribution, and accommodation, which are controlled by tectonic and climatic settings in the terrestrial realm (Flemings and Jordan, 1989; Paola et al., 1992). As Laramide deformation and the EECO both influenced the evolution of western North America during the early Eocene, discussion of allogenic controls on fluvial deposition in Main Canyon is warranted. Unfortunately the effect of hinterland tectonics on depositional variability in the southern Uinta Basin study area is difficult to assess as local tectonic uplifts are poorly constrained. Likewise, the timing and variation in the rate of tectonic subsidence of the lake basin is poorly understood. For the purpose of this study, we assume subsidence to be fairly linear although variation is undoubtedly likely.

Discussion of allogenic controls is further complicated by the fact that non-linearly related climate and tectonic controls produce similar external architectural stacking patterns (Armitage et al., 2011). For example, external fluvial geometry (e.g., height-width ratios) does not correlate to a specific climatic setting (e.g., humid) or tectonic regime (e.g., thermal subsidence, halokinesis, collision, rifting, or basin inversion) (Allen et al., 2013). However, the internal architecture of fluvial deposits is recognized to provide direct insight into climatically-controlled discharge and runoff regimes. Most notably, an abundance of UFR-structures like those observed in highly seasonal channels of Interval 1 indicates Froude supercritical flows with rapidly changing

flow velocity observed in seasonally-driven discharge regimes (McKee et al., 1967; Frostick and Reid, 1977; Tunbridge, 1984; Bromley, 1992; Alexander et al., 1999; Allen et al., 2013, 2014). While hinterland tectonics can affect continental climates and terrestrial runoff via rain shadow effects and drainage capture, the internal architecture of highly seasonal and perennial fluvial deposits in Main Canyon does indicate a stark change in fluvial discharge regimes.

Densely amalgamated fluvial deposits, such as those observed in Main Canyon Interval 1, have commonly been interpreted as a result of decreased tectonic subsidence and thereby decreased accommodation via the Leeder Allen Bridge (LAB) model (Allen, 1978; Leeder, 1978; Bridge and Leeder, 1979). For example, an extensively amalgamated fluvial sandstone body of the Willwood Formation, Bighorn Basin, WY, was first ascribed to slowed subsidence (Kraus, 1980). More recently, the high degree of amalgamation has been linked to rapid changes in river gradients related to oscillations in mean annual precipitation and/or to well-drained, sparsely vegetated floodplains (Foreman, 2014). Likewise, we relate the high degree of amalgamation observed in Interval 1 channels to repeated flooding events and avulsions as part of a highly seasonal fluvial system that is potentially part of a distributive fluvial fan system, rather than to changes in accommodation. Based on the lack of changes in channel stacking style through the interval, we infer little change in accommodation through the succession.

Paleogene fluvial deposition in the Western USA correlates with negative carbon isotopic excursions from the terrestrial record, suggesting fluvial expansion with hyperthermal warming events. This pattern is observed from PETM strata including the aforementioned Willwood Formation (Foreman, 2014) and the Wasatch Formation in the

Piceance Basin (Foreman et al., 2012), and from EECO strata including the GRF in the Greater Green River Basin (Aswasereelert et al., 2012; Smith et al., 2014) and the Tornillo Group in the Tornillo Basin, TX (Bataille et al., 2016). These continental fluvial expansions are interpreted to have occurred due to increased weathering rates and sediment transport associated with warmer, monsoonal climates induced by hyperthermal events (Smith et al., 2008, 2014; Hyland and Sheldon, 2013; Bataille et al., 2016).

Deposition of Main Canyon Interval 1 deposits is constrained between 54.0 Ma and 49.6 Ma (Figure 2), and is likely on the middle-younger side of this window based on the stratigraphic location of the C-Marker. These constraints and stratigraphic inferences suggest that Interval 1 coincides with the height of the EECO (ca. 52.6-50.1 Ma; Smith et al., 2014). Given fluvial expressions associated with hyperthermal events observed in similar western North America basins, we propose that the deposition of Interval 1 highly-seasonal fluvial deposits is directly linked to high-magnitude EECO hyperthermal events rather than to climatic variation altered by tectonic shifts (Figure 17). The hyperthermal events are likely responsible for a strong monsoonal sub-humid to semi-arid regional climate, which can explain the highly-variable discharge regime inferred from the preservation of UFR structures.

The shift from large UFR-dominated sandstone channels in lower Interval 1 to smaller, less laterally-extensive UFR-dominated sandstone channels in upper Interval 1 may represent the waning impact on seasonality of lower magnitude hyperthermal events that occurred later during the EECO (Figure 17; Zachos et al., 2001, 2010). The presence of larger heterolithic channels may further indicate less seasonal variation in precipition

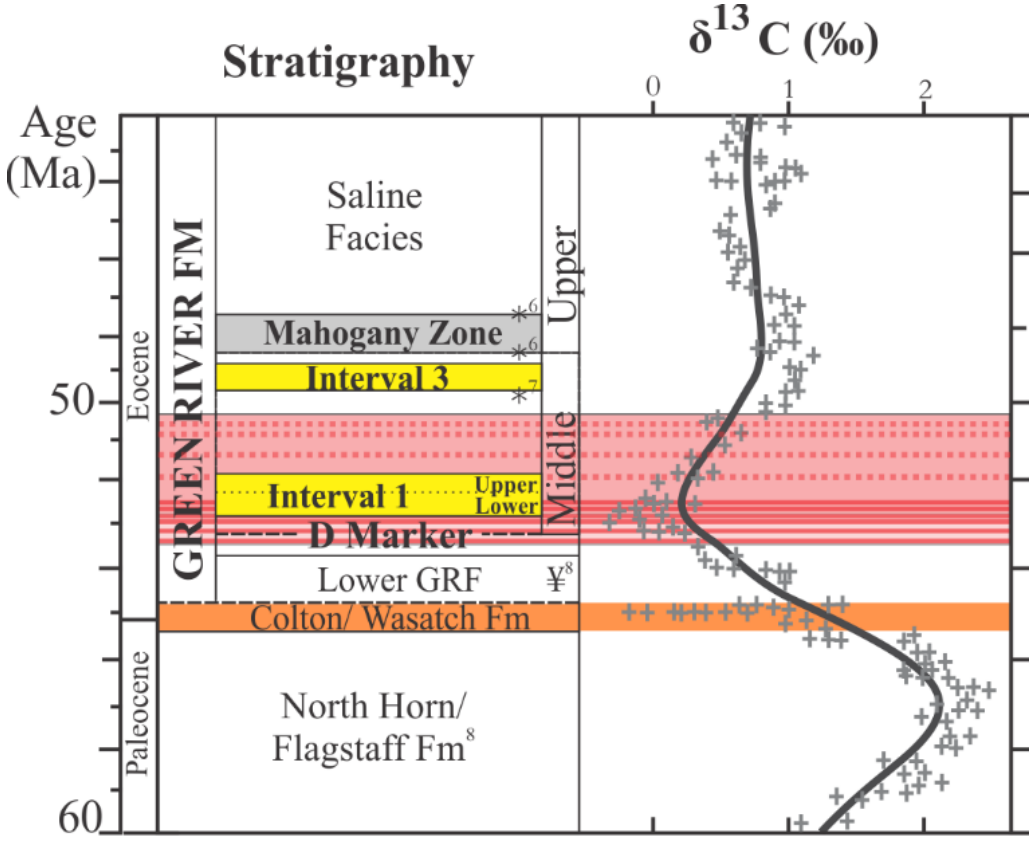

Figure 17. Summary interpretation of Main Canyon deposition with the EECO. See Figure 3 for complete compiled dataset and references.

and extended deposition under Froude subcritical flows, or perhaps that the main fluvial axis has avulsed elsewhere.

The overall rising base level of Lake Uinta observed over the vertical stratigraphy of Interval 1 may be a result of a highly seasonal climate regime that transports mass amounts of sediment and water into a closed basin or a result of tectonic subsidence. The changes in fluvial deposition from lower to upper Interval 1 could also be a direct result of the transgressing Lake Uinta, in which larger erosively-based heterolithic channels may be an artifact of nearshore fluvial deposition (Keighley et al., 2003), and seasonal storm sediment may have fluvial sediment that has been transported basinward via hyperpycnal flows (Bhattacharya and MacEachern, 2009; Schomacker et al., 2010). We interpret both allogenic factors, rising base level and a climatic setting, to be linked and have likely played a role in depositional variability from lower to upper Interval 1.

The lacustrine cyclicity observed in Interval 2 indicates broad repeated changes in sedimentary controls that may be allogenic or autogenic. For example, continued climate cyclicity of hyperthermal events could result in “warm-period” siliciclastic intervals that increase fluvial delivery of clastic sediment into the basin and carbonate intervals may represent “cool-periods” of relative fluvial quiescence, similar to interpretations made in the Greater Green River Basin (Smith et al., 2014). Alternatively, the cyclicity may represent regional migration of a fluvial source across a distributive fan system spanning the southern margin of Lake Uinta, which would allow thick carbonate accumulations in Main Canyon as fluvial input is active elsewhere in the basin. It is not likely that the cyclic changes are related to major base-level changes, as all lacustrine facies of Interval 2 display evidence for a shallow, littoral environment.

Unlike the laterally-extensive and amalgamated channels of Interval 1, Interval 3 channels tend to be less than several hundred meters wide, less amalgamated, and are more vertically and laterally-isolated from other channels. In the LAB model, this would suggest increased basin subsidence. However, the change in external geometry is interpreted to be related to a climatic shift that altered fluvial discharge and sediment delivery mechanism (Allen, 1978; Leeder, 1978; Bridge and Leeder, 1979). The trough cross bed-dominated expression of Interval 3 fluvial deposits indicates that (1) deposition occurred at relatively constant Froude subcritical velocities, or (2) if UFR-structures were formed, they were subsequently reworked into ripples and dunes in an active channel. Both situations inherently imply less discharge variability linked to a less variable climate (Allen et al., 2013, 2014; Plink-Björklund, 2015). Deposition of Interval 3 is constrained between 49.6 and 49.3 Ma, indicating that Interval 3 deposits occurred after the EECO and are within the Parachute Creek Member (Figure 2 & 3). Therefore, the perennial fluvial deposits of Interval 3 are a likely a result of a less seasonal continental climate and stable hydrologic regime of the post-EECO (Figure 17).

Fluvial expressions are recognized to change drastically in character over the distances they span (Blum and Tornqvist, 2000; Shukla et al., 2001; Jain and Sinha, 2004; Assine and Silva, 2009) and contextual facies suggest that lower Interval 3 is more nearshore than much of Interval 1 and upper Interval 1. However, the differences observed in the Interval 1 and Interval 3 fluvial deposits are not interpreted to represent downstream morphodynamic changes of the same fluvial system. In a distributary fluvial fan system, the distal reaches of the system may become more limited to smaller confined channels as flows are distributed and reduced (Donselaar et al., 2013). Confined

nearshore channels are observed as erosive heterolithic channels of upper Interval 1 and perennial channels of Interval 3. However, the sandstone expressions remain markedly different with UFR structures dominant in laterally-extensive channels in upper Interval 1 and trough cross strata dominant in confined channels of Interval 3. Outside of distributive fluvial fan setting, sediment transport associated with extreme seasonal flooding would be expected to transport mass amount of sediment throughout its course in increasingly centralized, high-discharge channels, and deposited under continued UFR conditions. As such, high deposition rates should characterize the downstream portions of the fluvial system as it interacts with the lake and loses sediment transport capacity (Fisher et al., 2007; Schomacker et al., 2010). Instead, more upstream Interval 1 displays evidence of high deposition rate features (like UFR structures), whereas nearshore Interval 3 records more stable deposition rates via dunes and oblique- to downstream-accreting macroforms, opposite of the predicted pattern. The two fluvial expressions are thereby interpreted to represent two distinct depositional regimes with different hydrologic controls. Broadly, we suggest a climatic change is visible in Main Canyon fluvial stratigraphy, from a highly seasonal climate of the peak EECO represented by siliciclastic flushing observed in the Douglas Creek Member in Interval 1, to less seasonal conditions of the post-EECO represented by stable discharge recorded in the Parachute Creek Member deposits of Interval 3.

CONCLUSIONS

Douglas Creek Member fluvial deposits of Interval 1 are characterized by weakly-channelized, amalgamated sandstone bodies that are laterally-extensive for 100s of meters to greater than a kilometer, 2-13.5 m thick, and dominated by UFR structures and bedforms, interpreted as flood deposits associated with a highly seasonal fluvial system. The fluvial deposits expand current highly seasonal fluvial facies models to include 1) clearly defined downstream accreting macroforms, and 2) the preservation of interbedded, erosively-based heterolithic channels that are 2-9 m thick and less than 350 m wide that are interpreted as dry season accumulations. The highly seasonal fluvial system is interpreted as a result of a semi-arid to sub-humid climate with monsoonally-driven fluvial flood discharge that led to rapid deposition of sand under Froude supercritical flow conditions in laterally-extensive channels. The aggradational fluvial system is identified as floodplain building, represented by thick accumulations of pedogenically modified siltstone and thick overbank sandstone deposits.

Parachute Creek Member fluvial deposits of Interval 3 are characterized as erosionally-based, isolated trough cross bed-dominated sandstone channels that extend laterally for 140-400 m, are up to 13 m thick, and are obliquely to downstream accreting, interpreted as a perennial fluvial system. Laterally adjacent facies consist of relatively thin floodplain deposits and lacustrine deposits, indicating a nearer Lake Uinta shoreline and limited floodplain building. Perennial fluvial deposits are interpreted to represent the

continuous erosion and deposition in a less seasonally-controlled climate in a braided to meandering stream environment, akin to typical fluvial facies of mid-latitude, perennial fluvial systems of temperate North America.

The progression of fluvial deposits from a seasonally-controlled fluvial regime to a perennial regime indicates different controls on fluvial deposition through the early Eocene, interpreted as a fundamental shift in climate. Highly seasonal fluvial deposits of Interval 1 are interpreted to coincide with the peak EECO, in which hyperthermal events resulted in a monsoonal continental climate that led to a fluvial system that experienced extreme seasonal variation in discharge. As the hyperthermal-dominated regime waned and became absent during the post-EECO, fluvial discharge became less seasonally driven as represented by Interval 3. The variability of Douglas Creek and Parachute Creek Member deposits highlights the evolution of marginal Lake Uinta with Eocene climate and further iterates the importance and utility of multiple fluvial facies models for climatic interpretation.

APPENDIX

XRD METHODS AND RESULTS

Nine fine-grained facies from TB section were characterized using whole rock and clay X-ray diffraction (XRD) to aid facies analysis. Fine-grained samples were powdered, and bulk and clay-sized analyses were performed using a Bruker D8 Advance X-ray diffactometer at the Energy & Geoscience Institute located in Salt Lake City, UT. The Rietvield method was used for phase quantification using TOPAS software developed by Bruker AXS, which fits the peak intensities calculated from modeled crystalline structure to the observed X-ray powder pattern by a least squares refinement. This is done by varying crystal structure parameters to minimize the difference between calculated and observed powder patterns.

The following operating parameters were used in sample analysis: Cu-K-α radiation at 40 kV and 40 mA, 0.02º2θ step size, and 0.4 and 0.6 seconds per step, for clay and bulk samples, respectively. Clay samples were examined from 2 to 45º2θ, and the bulk samples from 4 to 65º2θ. The instrument is equipped with a Lynx Eye detector that collects data over 2.6 mm. At least three analyses were conducted on each sample, two or more on the clay-sized fraction and one on the bulk sample. Clay-sized fraction identification follows methodology by Moore and Reynolds (1997). Results are compiled in Table 3.

Table 3. Bulk X-ray diffraction results by sample with facies association

Sample	Illite	Chlorite	Kaolinite	Smectite	Vermiculite	Plagioclase	K-Feldspar	Quartz	Calcite	Dolomite	Analcime
TB-002 (FA2.2)	6	9	6			18	20	29			12
TB-006 (FA3.1)	3	14	6			15	19	17	2	1	26
TB-013 (FA3.3)	5	11	6			17	15	15	7	10	14
TB-022 (FA3.2)	2	8	6			23	17	31	6	2	6
TB-027 (FA3.6)	6	4	4	tr		18	15	33	6	4	10
TB-037 (FA3.6)	8	19	8			12	20	12	tr	tr	22
TB-052 (FA1.2)	3	7	5			21	19	28	8	3	6
TB-058 (FA3.3)	3	10	5		tr	16	21	26	4	1	15
TB-092 (FA3.6)	4	8	10	tr		15	26	29	3	4	2
TB-102 (FA3.1)	4	19	8	tr		13	24	14	3	tr	15

Note: Mineral abundances are given in weight percent of the sample, with results rounded to the nearest whole number. Fields marked with tr (trace) indicate that mineral is present, but that its abundance calculated from the Rietveld refinement was less than one weight percent and/or it was observed in the clay-sized fraction, but not the bulk sample.

REFERENCES

Abbott, W., 1957, Tertiary of the Uinta Basin, in Seal, O.G. ed., Guidebook to the Geology of the Uinta Basin: Eight Annual Field Conference, p. 102–109.

Abdullatif, O.M., 1989, Channel-fill and sheet-flood facies sequences in the ephemeral terminal River Gash, Kassala, Sudan: Sedimentary Geology, v. 63, p. 171–184, doi: 10.1016/0037-0738(89)90077-8.

Abels, H.A., Clyde, W.C., Gingerich, P.D., Hilgen, F.J., Fricke, H.C., Bowen, G.J., and Lourens, L.J., 2012, Terrestrial carbon isotope excursions and biotic change during Palaeogene hyperthermals: Nature Geoscience, v. 5, p. 326–329, doi: 10.1038/ngeo1427.

Alexander, J., 2008, Bedforms in Froude-supercritical flow: Marine and River Dune Dynamics Proceedings, p. 1–5, http://www.shom.fr/fr_page/fr_act_geo/abstract2008/a0_Alexander.pdf.

Alexander, J., Bridge, J.S., Cheela, R.J., and Leclair, S.F., 2001, Bedforms and associated sedimentary structures formed undersupercritical waterfows over aggrading sand beds: Sedimentology, v. 48, p. 133–152.

Alexander, J., Fielding, C.R., and Pocock, G.D., 1999, Flood behaviour of the Burdekin River, tropical north Queensland, Australia: Geological Society, London, Special Publications, v. 163, p. 27–40.

Allen, J.R.L., 1965, A review of the origin and characteristics of recent alluvial sediments: Sedimentology, v. 5, p. 89–191.

Allen, J.R.L., 1984, Development in sedimentology 30: Sedimentary structures their character and physical basis: Elsevier Science, Inc., 663 p.

Allen, J.R.L., 1973, Features of cross-stratified units due to random and other changes in bed forms: Sedimentology, v. 20, p. 189–202.

Allen, J.R.L., 1974, Reaction, relaxation and lag in natural sedimentary systems: general principles, examples and lessons: Earth-Science Reviews, v. 10, p. 263–342.

Allen, J.R.L., 1978, Studies in fluviatile sedimentation: an exploratory quantitative model for the architecture of avulsion-controlled alluvial suites: Sedimentary Geology, v. 21, p. 129–147.

Allen, J.P., Fielding, C.R., Gibling, M.R., and Rygel, M.C., 2014, Recognizing products of palaeoclimate fluctuation in the fluvial stratigraphic record: An example from the Pennsylvanian to Lower Permian of Cape Breton Island, Nova Scotia: Sedimentology, v. 61, p. 1332–1381, doi: 10.1111/sed.12102.

Allen, J.P., Fielding, C.R., Rygel, M.C., and Gibling, M.R., 2013, Deconvolving Signals of Tectonic and Climatic Controls From Continental Basins: An Example From the Late Paleozoic Cumberland Basin, Atlantic Canada: Journal of Sedimentary Research, v. 83, p. 847–872, doi: 10.2110/jsr.2013.58.

Alonso-Zarza, A.M., 2003, Palaeoenvironmental significance of palustrine carbonates and calcretes in the geological record: Earth-Science Reviews, v. 60, p. 261–298.

Armitage, J.J., Duller, R.A., Whittaker, A.C., and Allen, P.A., 2011, Transformation of tectonic and climatic signals from source to sedimentary archive: Nature Geoscience, v. 4, p. 231–235, doi: 10.1038/ngeo1087.

Ashworth, P.J., 1996, Mid-channel bar growth and its relationship to local flow strength and direction: Earth Surface Processes and Landforms, v. 21, p. 103–123, doi: Doi 10.1002/(Sici)1096-9837(199602)21:2<103::Aid-Esp569>3.0.Co;2-O.

Assine, M.L., and Silva, A., 2009, Contrasting fluvial styles of the Paraguay River in the northwestern border of the Pantanal wetland, Brazil: Geomorphology, v. 113, p. 189–199, doi: 10.1016/j.geomorph.2009.03.012.

Awramik, S.M., and Buchheim, H.P., 2015, Giant stromatolites of the Eocene Green River Formation: Geology, v. 43, p. 691–694, doi: 10.1130/G36793.1.

Bataille, C.P., Watford, D., Ruegg, S., Lowe, A., and Bowen, G.J., 2016, Chemostratigraphic age model for the Tornillo Group: A possible link between fluvial stratigraphy and climate: Palaeogeography, Palaeoclimatology, Palaeoecology, v. 457, p. 277–289, doi: 10.1016/j.palaeo.2016.06.023.

Bhattacharya, J.P., and MacEachern, J.A., 2009, Hyperpycnal rivers and prodeltaic shelves in the Cretaceous seaway of North America: Journal of Sedimentary Research, v. 79, p. 184–209, doi: 10.2110/jsr.2009.026.

Blackett, R.E., 1996, Tar-sand resources of the Uinta Basin, Utah: 122 p., http://ugspub.nr.utah.gov/publications/open_file_reports/OFR-335.pdf.

Blodgett, R.H., and Stanley, K.O., 1980, Stratification, bedforms, and discharge relations of the Platte braided river system, Nebraska: Journal of Sedimentary Research, v. 50.

Blum, M.D., and Tornqvist, T.E., 2000, Fluvial responses to climate and sea-level change : a review and look forward: Sedimentology, v. 47, p. 2–48.

Bohacs, K.M., Carroll, A.R., Neal, J.E., and Mankiewicz, P.J., 2000, Lake-Basin Type, Source Potential, and Hydrocarbon Character: An Integrated Sequence-Stratigraphic-Geochemical Framework, in Gierlowski-Kordesch, E.H. and Kelts,

K.R. eds., Lake Basins Through Space and Time, AAPG Studies in Geology 46, p. 3–34, doi: http://dx.doi.org/10.1306/E4FD42AB-1732-11D7-8645000102C1865D.

Bown, T.M., and Kraus, M.J., 1987, Integration of Channel and Floodplain Suites , Developmental Sequence and Lateral Relations of Alluvial Paleosols: Journal of Sedimentary Petrology, v. 57, p. 587–601.

Bradley, W.H., 1931, Origin and microfossils of the oil shale of the Green River Formation of Colorado and Utah: Utah Geological Survey Professional Paper, v. 168, 1-58 p.

Bridge, J.S., 1993, Description and interpretation of fluvial deposits: a critical perspective: Sedimentology, v. 40, p. 801–810.

Bridge, J.S., and Leeder, M.R., 1979, A simulation model of alluvial stratigraphy: Sedimentology, v. 26, p. 617–644.

Bridge, J.S., and Lunt, I.A., 2006, Depositional models of braided rivers: Braided Rivers, Processes, Deposits, Ecology and Management, Int. Assoc. Sediment. Spec. Pub, v. 36, p. 11–51.

Bromley, M.H., 1992, Ephemeral and Perennial Fluvial Processes, in Miall, A.D. and Tyler, N. eds., The Three-Dimensional Facies Architecture of Terrigenous Clastic Sediments and Its Implications for Hydrocarbon Discovery and Recovery (CSP3), p. 94–102.

Bryant, M., Falk, P., and Paola, C., 1995, Experimental study of avulsion frequency and rate of deposition: Geology, v. 23, p. 365–368, doi: 10.1130/0091-7613(1995)023<0365:ESOAFA>2.3.CO.

Bunde, A., Eichner, J.F., Kantelhardt, J.W., and Havlin, S., 2005, Long-Term Memory : A Natural Mechanism for the Clustering of Extreme Events and Anomalous Residual Times in Climate Records: Physical Review Letters, v. 94, p. 1–4, doi: 10.1103/PhysRevLett.94.048701.

Burst, J.F., 1976, Argillaceous sediment dewatering: Annual Review of Earth and Planetary Sciences, v. 4, p. 293.

Cant, D.J., and Walker, R.G., 1976, Development of a braided-fluvial facies model for the Devonian Battery Point Sandstone, Quebec: Canadian Journal of Earth Sciences, v. 13, p. 102–119.

Carroll, A.R., Sciences, G., and Street, W.D., 1999, Stratigraphic classification of ancient lakes : Balancing tectonic and climatic controls: Geology, v. 27, p. 99–102.

Cashion, W.B., 1967, Geology and fuel resources of the Green River Formation, southeastern Uinta Basin, Utah and Colorado: U.S. Geological Survey Professional Paper 548, p. 48.

Cater, F.W., 1966, Age of the Uncompahgre uplift and Unaweep Canyon, west-central Colorado: US Geological Survey Professional Paper 550, p. C86–C92.

Chakraborty, T., and Ghosh, P., 2010, The geomorphology and sedimentology of the Tista megafan, Darjeeling Himalaya: Implications for megafan building processes: Geomorphology, v. 115, p. 252–266, doi: 10.1016/j.geomorph.2009.06.035.

Chakraborty, T., Kar, R., Ghosh, P., and Basu, S., 2010, Kosi megafan: Historical records, geomorphology and the recent avulsion of the Kosi River: Quaternary International, v. 227, p. 143–160, doi: 10.1016/j.quaint.2009.12.002.

Clyde, W.C., Sheldon, N.D., Koch, P.L., Gunnell, G.F., and Bartels, W.S., 2001, Linking the Wasatchian/Bridgerian boundary to the Cenozoic Global Climate Optimum: new magnetostratigraphic and isotopic results from South Pass, Wyoming: Palaeogeography, Palaeoclimatology, Palaeoecology, v. 167, p. 175–199.

Cramer, B.S., Wright, J.D., Kent, D. V, and Aubry, M., 2003, Orbital climate forcing of D13C excursions in the late Paleocene – early Eocene (chrons C24n-C25n): Paleoceanography, v. 18, p. 1–25, doi: 10.1029/2003PA000909.

Dane, C.H., 1954, Stratigraphic and facies relationships of upper part of Green River Formation and lower part of Uinta Formation in Duchesne, Uintah, and Wasatch counties, Utah: AAPG Bulletin, v. 38, p. 405–425.

Das, P.K., 1986, Monsoons: New Delhi National Book Trust, India, 162 p.

Davis, S.J., Dickinson, W.R., Gehrels, G.E., Spencer, J.E., Lawton, T.F., and Carroll, A.R., 2010, The Paleogene California River: Evidence of Mojave-Uinta paleodrainage from U-Pb ages of detrital zircons: Geology, v. 38, p. 931–934, doi: 10.1130/G31250.1.

Díaz Granados, M.A., Valdes, J.B., and Bras, R.L., 1984, A physically based flood frequency distribution: Water Resources Research, v. 20, p. 995–1002.

Dickinson, W.R., Lawton, T.F., and Inman, K.F., 1986, Sandstone detrital modes, central Utah foreland region: stratigraphic record of Cretaceous-Paleogene tectonic evolution: Journal of Sedimentary Petrology, v. 56, p. 276–293.

Dickinson, W.R., Klute, M.A., Hayes, M.J., Janecke, S.U., Lundin, E.R., McKittrick, M.A., and Olivares, M.D., 1988, Paleogeographic and paleotectonic setting of Laramide sedimentary basins: Geological Society of America Bulletin, v. 100, p. 1023–1039.

Donselaar, M.E., Cuevas Gozalo, M.C., and Moyano, S., 2013, Avulsion processes at the terminus of low-gradient semi-arid fluvial systems: Lessons from the Rio Colorado, Altiplano endorheic basin, Bolivia: Sedimentary Geology, v. 283, p. 1–14, doi: 10.1016/j.sedgeo.2012.10.007.

Driese, S.G., and Ober, E.G., 2005, Paleopedological and paleohydrologic records of precipitation seasonality from early Pennsylvanian “underclay” paleosols, U.S.A.: Journal of Sedimentary Research, v. 75, p. 997–1010.

Eagleson, P.S., 1972, Dynamics of flood frequency: Water Resources Research, v. 8, p. 878–898.

Fielding, C.R., 2006, Upper flow regime sheets, lenses and scour fills: Extending the range of architectural elements for fluvial sediment bodies: Sedimentary Geology, v. 190, p. 227–240, doi: 10.1016/j.sedgeo.2006.05.009.

Fielding, C.R., Alexander, J., and Newman-Sutherland, E., 1997, Preservation of in suite, arborscent vegetation and fluvial bar construction in the Burdekin River of north Queensland , Australia: Palaeogeography, Palaeoclimatology, Palaeoecology, v. 35, p. 123–144.

Fielding, C.R., Allen, J.P., Alexander, J., and Gibling, M.G., 2009, Facies model for fluvial systems in the seasonal tropics and subtropics: Geology, v. 37, p. 623–626, doi: 10.1130/G25727A.1.

Fielding, C.R., Allen, J.P., Gibling, M.R., Rygel, M.C., and Calder, J.H., 2011, Fluvial systems and their deposits in hot, seasonal semiarid and subhumid settings: modern and ancient examples, in From River to Rock Record: The Preservation of Fluvial Sediments and their Subsequent Interpretation, p. 89–111.

Fisher, J.A., Nichols, G.J., and Waltham, D.A., 2007, Unconfined flow deposits in distal sectors of fluvial distributary systems: Examples from the Miocene Luna and Huesca Systems, northern Spain: Sedimentary Geology, v. 195, p. 55–73, doi: 10.1016/j.sedgeo.2006.07.005.

Flemings, P.B., and Jordan, T.E., 1989, A synthetic stratigraphic model of foreland basin development: Journal of Geophysical Research, v. 94, p. 3851–3866.

Ford, G.L., and Pyles, D.R., 2014, A hierarchical approach for evaluating fluvial systems: Architectural analysis and sequential evolution of the high net-sand content, middle Wasatch Formation, Uinta Basin, Utah: AAPG Bulletin, v. 98, p. 1273–1304, doi: 10.1306/12171313052.

Foreman, B.Z., 2014, Climate-driven generation of a fluvial sheet sand body at the Paleocene-Eocene boundary in north-west Wyoming (USA): Basin Research, v. 26, p. 225–241, doi: 10.1111/bre.12027.

Foreman, B.Z., Heller, P.L., and Clementz, M.T., 2012, Fluvial response to abrupt global warming at the Palaeocene/Eocene boundary.: Nature, v. 491, p. 92–5, doi: 10.1038/nature11513.

Fouch, T.D., 1975, Lithofacies and related hydrocarbon accumulations in Tertiary strata of the western and central Uinta basin, Utah: Rocky Mountain Association of Geologists - 1975 Symposium, p. 163–173.

Fouch, T.D., Hanley, J.H., Forester, R.M., Keighin, C.W., Pitman, J.K., and Nichols, D.J., 1987, Chart showing lithology, mineralogy, and paleontology of the nonmarine North Horn Formation and Flagstaff Member of the Green River Formation, Price Canyon, central Utah - A principal reference section: U.S.Geological Survey Miscellaneous InvestigationSeries Map I–1797–A, p. 1.

Frantz, C.M., Petryshyn, V.A., Marenco, P.J., Tripati, A., Berelson, W.M., and Corsetti, F.A., 2014, Dramatic local environmental change during the Early Eocene Climatic Optimum detected using high resolution chemical analyses of Green River Formation stromatolites: Palaeogeography, Palaeoclimatology, Palaeoecology, v. 405, p. 1–15, doi: 10.1016/j.palaeo.2014.04.001.

Frostick, L.E., and Reid, I., 1977, The origin of horizontal laminae in ephemeral stream channel-fill: Sedimentology, v. 24, p. 1–9.

Galloway, W.E., and Hobday, D.K., 1996, Terrigenous Clastic Depositional Systems : Applications to Fossil Fuel and Groundwater Resources: Springer, 489 p.

Hajek, E.A., and Edmonds, D.A., 2014, Is river avulsion style controlled by floodplain morphodynamics? Geology, v. 42, p. 199–202, doi: 10.1130/G35045.1.

Hickin, E.J., 1993, Fluvial facies models : a review of Canadian research: Progress in Physical Geography, v. 17, p. 205–222, doi: 10.1177/030913339301700207.

Hren, M.T., Pagani, M., Erwin, D.M., and Brandon, M.T., 2010, Biomarker reconstruction of the early Eocene paleotopography and paleoclimate of the northern Sierra Nevada: Geology, v. 38, p. 7–10, doi: 10.1130/G30215.1.

Horn, J.D., Fielding, C.R. and Joeckel, R.M., 2012. Revision of Platte River alluvial facies model through observations of extant channels and barforms, and subsurface alluvial valley fills: Journal of Sedimentary Research, v. 82, pp.72-91.

Hyland, E.G., and Sheldon, N.D., 2013, Coupled CO2-climate response during the Early Eocene Climatic Optimum: Palaeogeography, Palaeoclimatology, Palaeoecology, v. 369, p. 125–135.

Hyland, E.G., Sheldon, N.D., and Fan, M., 2013, Terrestrial paleoenvironmental reconstructions indicate transient peak warming during the early Eocene climatic optimum: Geological Society of America Bulletin, v. 125, p. 1338–1348, doi: 10.1130/B30761.1.

Jain, V., and Sinha, R., 2004, Fluvial dynamics of an anabranching river system in Himalayan foreland basin, Baghmati river, north Bihar plains, India: Geomorphology, v. 60, p. 147–170, doi: 10.1016/j.geomorph.2003.07.008.

Johnson, R.C., 1985, Early Cenozoic history of the Uinta and Piceance Creek basins, Utah and Colorado, with special reference to the development of Eocene Lake Uinta, in Flores, R.M. and Kaplan, S.S. eds., Cenozoic Paleogeography of the West-Central United States, Rocky Mountain Section (SEPM), p. 247–276.

Johnson, R.C., Mercier, T.J., Brownfield, M.E., Self, J.G., Ryder, R.T., Michael, E., and Self, J.G., 2011, Assessment of In-Place Oil Shale Resources of the Eocene Green River Formation, Greater Green River Basin, Wyoming, Colorado, and Utah, in Oil shale resources of the Eocene Green River Formation, Greater Green River Basin, Wyoming, Colorado, and Utah, p. 1–60.

Keighley, D., Flint, S., Howell, J., and Moscariello, A., 2003, Sequence stratigraphy in lacustrine basins: a model for part of the Green River Formation (Eocene), southwest Uinta Basin, Utah, U.S.A: Journal of Sedimentary Research, v. 73, p. 987–1006.

Kesel, R.H., Yodis, E.G., and McCraw, D.J., 1992, An approximation of the sediment budget of the lower Mississippi River prior to major human modification: Earth Surface Processes and Landforms, v. 17, p. 711–722.

Kraus, M.J., 1980, Genesis of a fluvial sheet sandstone, Willwood Formation, Northwest Wyoming, in Gingerich, P.D. ed., Early Cenozoic Paleontology and Stratigraphy of the Bighorn Basin, Wyoming, p. 87–94.

Kraus, M.J., 1999, Paleosols in clastic sedimentary rocks : their geologic applications: Earth-Science Reviews, v. 47, p. 41–70.

Kumar, R., 1993, Coalescence megafan: multistorey sandstone complex of the late-orogenic (Mio-Pliocene) sub-Himalayan belt, Dehra Dun, India: Sedimentary geology, v. 85, p. 327–337.

Kumar, R., Ghosh, S.K., Mazari, R.K., and Sangode, S.J., 2003, Tectonic impact on the fluvial deposits of Plio-Pleistocene Himalayan foreland basin, India: Sedimentary Geology, v. 158, p. 209–234, doi: 10.1016/S0037-0738(02)00267-1.

Kumar, R., and Tandon, S.K., 1985, Sedimentology of Plio-Pleistocene Late orogenic deposits associated with intraplate subduction—the Upper Siwalik Subgroup of a part of Panjab Sub-Himalaya, India: Sedimentary Geology, v. 42, p. 105–158.

Langford, R., and Bracken, B., 1987, Medano Creek, Colorado, a model for upper-flow-regime fluvial deposition: Journal of Sedimentary Petrology, v. 57, p. 863–870.

Lawton, T.F., 2008, Laramide sedimentary basins, in Miall, A.D. ed., Sedimentary Basins of the World, Elsevier, v. 5, p. 429–450, doi: http://dx.doi.org/10.1016/S1874-5997(08)00012-9.

Leeder, M.R., 1978, A quantitative stratigraphic model for allu- vium, with special reference to channel deposit density and interconnectedness, in Miall, A.D. ed., Fluvial Sedimentology, Can. Soc. Petrol. Geol., Mem., 5, p. 587–596.

Leier, A.L., Decelles, P.G., and Pelletier, J.D., 2005, Mountains, monsoons, and megafans: Geological Society, London, Special Publications, v. 33, p. 289–292, doi: 10.1130/G21228.1.

Lourens, L.J., Sluijs, A., Kroon, D., Zachos, J.C., Thomas, E., Röhl, U., Bowles, J., and Raffi, I., 2005, Astronomical pacing of late Palaeocene to early Eocene global warming events: Nature, v. 435, p. 1083–1087, doi: 10.1038/nature03814.

Machette, M.N., 1985, Calcic soils of the southwestern United States: Geological Society of America Special Papers 203, p. 1–22.

McCarthy, P.J., and Plint, A.G., 1998, Recognition of interfluve sequence boundaries : Integrating paleopedology and sequence stratigraphy: Geology, v. 26, p. 387–390.

McGlue, M.M., Soreghan, M.J., Michel, E., Todd, J.A., Cohen, A.S., Mischler, J., O'Connel, C.S., Castaneda, O.S., Hartwell, R.J., Lezzar, K.E., and Nkotagu, H.H., 2010, Environmental Controls on Shell-Rich Facies in Tropical Lacustrine Rifts: a View From Lake Tanganyika'S Littoral: Palaios, v. 25, p. 426–438, doi: 10.2110/palo.2009.p09-160r.

McKee, E.D., Crosby, E.J. t, and Berryhill Jr, H.L., 1967, Flood deposits, Bijou Creek, Colorado, June 1965: Journal of Sedimentary Research, v. 37.

McNeill, D.F., Cunningham, K.J., Guertin, L. a, and Anselmetti, F.S., 2004, Depositional themes of mixed carbonate-siliciclastics in the South Florida Neogene; application to ancient deposits: AAPG Memoir, v. 80, p. 23–43, http://search.ebscohost.com/login.aspx?direct=true&db=geh&AN=2005-049146&site=ehost-live.

Miall, A.D., 1978, Lithofacies types and vertical profile models in braided river deposits: a summary: Fluvial Sedimentology, v. 5, p. 597–600.

Miall, A.D., 2013, The geology of fluvial deposits: sedimentary facies, basin analysis, and petroleum geology: Springer, 582 p.

Mills, P.C., 1983, Genesis and diagnostic value of soft-sediment deformation structures—a review: Sedimentary Geology, v. 35, p. 83–104.

Milroy, P.G., and Wright, V.P., 2002, Fabrics, facies control and diagenesis of lacustrine ooids and associated grains from the Upper Triassic, southwest England: Geological Journal, v. 37, p. 35–53.

Mohrig, D., Heller, P.L., and Lyons, W.J., 2000, Guadalope-Matarranya system (northern Spain) and Wasatch Formation (western Colorado): Geological Soceity of America Bulletin, v. 112, p. 1787–1803, doi: 10.1130/0016-7606(2000)112<1787:IAPFAA>2.0.CO;2.

Moore, J., Taylor, A., Johnson, C., Ritts, B.D., and Archer, R., 2012, Facies Analysis, Reservoir Characterization, and LIDAR Modeling of an Eocene Lacustrine Delta, Green River Formation, Southwest Uinta Basin, Utah, in Baganz, O.W., Bartov, Y., Bohacs, K.M., and Nummedal, D. eds., Lacustrine sandstone reservoirs and hydrocarbon systems: AAPG Memoir 95, p. 183–208, doi: 10.1306/13291389M953449.

Morgan, C.D., Chidsey, T.C., McClure, K.P., Bereskin, S.R., and Deo, M.D., 2003, Reservoir characterization of the Lower Green River Formation, Uinta Basin, Utah.:

Mount, J.F., 1984, Mixing of siliciclastic and carbonate sediments in shallow shelf environments.: Geology, v. 12, p. 432–435, doi: 10.1130/0091-7613(1984)12<432:MOSACS>2.0.CO.

Myrow, P., 1990, A New Graph For Understanding Colors of Mudrocks: Journal of Geological Education, v. 38, p. 16–20.

Nicholas, A.P., Sambrook Smith, G.H., Amsler, M.L., Ashworth, P.J., Best, J.L., Hardy, R.J., Lane, S.N., Orfeo, O., Parsonsm, D.R., Reesink, A.J.H., Sandbach, S.D., Simpson, C.J., and Szupiany, R.N., 2016, The role of discharge variability in determining alluvial stratigraphy: Geology, v. 44, p. 3–6, doi: 10.1130/G37215.1.

Nichols, G.J., and Fisher, J.A., 2007, Processes, facies and architecture of fluvial distributary system deposits: Sedimentary Geology, v. 195, p. 75–90, doi: 10.1016/j.sedgeo.2006.07.004.

Nicolo, M.J., Dickens, G.R., Hollis, C.J., and Zachos, J.C., 2007, Multiple early Eocene hyperthermals: Their sedimentary expression on the New Zealand continental margin and in the deep sea: Geology, v. 35, p. 699–702, doi: 10.1130/G23648A.1.

Olariu, C., and Bhattacharya, J.P., 2006, Terminal distributary channels and delta front architecture of river-dominated delta systems: Journal of Sedimentary Research, v. 76, p. 212–233, doi: 10.2110/jsr.2006.026.

Osmond, J.C., 1964, Tectonic history of the Uinta basin, Utah, in Guidebook to the Geology and Mineral Resources of the Uinta Basin: Utah's Hydrocarbon Storehouse, Intermountain Association of Petroleum Geologists 13th Annual Field Conference Guidebook, Utah Geological Association.

Paola, C., Heller, P.L., and Angevine, C.L., 1992, The large-scale dynamics of grain-size variation in alluvial basins, 1: Theory: Basin Research, v. 4, p. 73–90.

Pitman, J.K., Fouch, T.D., and Goldhaber, M.B., 1982, Depositional setting and diagenetic evolution of some Tertiary unconventional reservoir rocks, Uinta Basin, Utah.: American Association of Petroleum Geologists Bulletin, v. 66, p. 1581–1596.

Plink-Björklund, P., 2015, Morphodynamics of rivers strongly affected by monsoon precipitation: Review of depositional style and forcing factors: Sedimentary Geology, v. 323, p. 110–147, doi: 10.1016/j.sedgeo.2015.04.004.

Quesne, D., Buta-Neto, A., Benard, D., and Guiraud, M., 2009, Distribution of Albian clastic deposits in the Benguela basin (Angola): Evidence of a Benguela palaeocurrent? Bulletin de la Societe Geologique de France, v. 180, p. 117–129, doi: 10.2113/gssgfbull.180.2.117.

Remy, R.R., 1992, Stratigraphy of the Eocene part of the Green River Formation in the south-central part of the Uinta Basin, Utah: U.S. Geological Survey Bulletin, Volume 1787-BB, p. 1–79, papers2://publication/uuid/832AF5DF-D7FE-403C-AC37-D74C0836301B.

Rosencrans, E.M., 2015, Stratigraphic architecture of deltaic mouthbar deposits during the Early Eocene Climatic Optimum, Green River Formation, Uinta Basin, Utah: Master's Thesis, University of Utah, Salt Lake City, Utah, 146 p.

Schomacker, E.R., Kjemperud, A.V., Petter, J., Ystuen, N., and Jahren, J.S., 2010, Recognition and significance of sharp-based mouth-bar deposits in the Eocene Green River Formation, Uinta Basin, Utah: Sedimentology, v. 57, p. 1069–1087, doi: 10.1111/j.1365-3091.2009.01136.x.

Sewall, J.O., and Sloan, L.C., 2006, Come a little bit closer : A high-resolution climate study of the early Paleogene Laramide foreland: Geology, v. 34, p. 81–84, doi: 10.1130/G22177.1.

Sexton, P.F., Wilson, P. a., and Norris, R.D., 2006, Testing the Cenozoic multisite composite δ 18 O and δ 13 C curves: New monospecific Eocene records from a single locality, Demerara Rise (Ocean Drilling Program Leg 207): Paleoceanography, v. 21, p. PA2019, doi: 10.1029/2005PA001253.

Shellito, C.J., Sloan, L.C., and Huber, M., 2003, Climate model sensitivity to atmospheric CO 2 levels in the Early-Middle Paleogene: Palaeogeography, Palaeoclimatology, Palaeoecology, v. 193, p. 113–123, doi: 10.1016/S0031-0182(02)00718-6.

Shukla, U.K., Singh, I.B., Sharma, M., and Sharma, S., 2001, A model of alluvial megafan sedimentation: Ganga Megafan: Sedimentary Geology, v. 144, p. 243–262, doi: 10.1016/S0037-0738(01)00060-4.

Singh, A., and Bhardwaj, B.D., 1991, Fluvial facies model of the Ganga River sediments, India: Sedimentary Geology, v. 72, p. 135–146.

Skelly, R.L., Bristow, C.S., and Ethridge, F.G., 2003, Architecture of channel-belt deposits in an aggrading shallow sandbed braided river: The lower Niobrara River, northeast Nebraska: Sedimentary Geology, v. 158, p. 249–270, doi: 10.1016/S0037-0738(02)00313-5.

Smith, D.G., 1987, Meandering river point bar lithofacies models: modern and ancient examples compared: The Society of Economic Paleontologists and Mineralogists, v. 39, p. 83–91.

Smith, M.E., and Carroll, A.R. (Eds.), 2015, Stratigraphy and paleolimnology of the Green River Formation, Western USA: Heidelberg, Springer, 350 p.

Smith, M.E., Singer, B.S., Carroll, A.R., and Fournelle, J.H., 2006, High-resolution calibration of Eocene strata : 40 Ar / 39 Ar geochronology of biotite in the Green River Formation: Geology, v. 34, p. 393–396, doi: 10.1130/G22265.1.

Smith, M.E., Carroll, A.R., and Mueller, E.R., 2008, Elevated weathering rates in the Rocky Mountains during the Early Eocene Climatic Optimum: Nature Geoscience, v. 1, p. 370–374, doi: 10.1038/ngeo205.

Smith, M.E., Carroll, A.R., and Singer, B.S., 2008, Synoptic reconstruction of a major ancient lake system : Eocene Green River Formation, western United States: GSA Bulletin, v. 120, p. 54–84, doi: 10.1130/B26073.1.

Smith, M.E., Chamberlain, K.R., Singer, B.S., and Carroll, A.R., 2010, Eocene clocks agree : Coeval 40 Ar / 39 Ar , U-Pb , and astronomical ages from the Green River Formation: Geology, v. 38, p. 527–530, doi: 10.1130/G30630.1.

Smith, M.E., Carroll, A.R., Scott, J.J., and Singer, B.S., 2014, Early Eocene carbon isotope excursions and landscape destabilization at eccentricity minima: Green River Formation of Wyoming: Earth and Planetary Science Letters, v. 403, p. 393–406, doi: 10.1016/j.epsl.2014.06.024.

Stanley, K.O., and Collinson, J.W., 1979, Depositional history of Paleocene-Lower Eocene Flagstaff Limestone and coeval rocks, central Utah: AAPG Bulletin, v. 63, p. 311–323.

Subyani, A.M., 2009, Hydrologic behavior and flood probability for selected arid basins in Makkah area, western Saudi Arabia: Arabian Journal of Geosciences, v. 4, p. 817–824, doi: 10.1007/s12517-009-0098-1.

Tänavsuu-Milkeviciene, K., and Sarg, F.J., 2012. Evolution of an organic-rich lake basin–stratigraphy, climate and tectonics: Piceance Creek basin, Eocene Green River Formation: Sedimentology, v. 59, p.1735-1768.

Taylor, A.W., and Ritts, B.D., 2004, Mesoscale heterogeneity of fluvial-lacustrine reservoir analogues: Examples from the Eocene Green River and Colton Formations, Uinta Basin, Utah, USA: Journal of Petroleum Geology, v. 27, p. 3–26, doi: 10.1111/j.1747-5457.2004.tb00042.x.

Therrien, F., 2005, Palaeoenvironments of the latest Cretaceous (Maastrichtian) dinosaurs of Romania: Insights from fluvial deposits and paleosols of the Transylvanian and Haţeg basins: Palaeogeography, Palaeoclimatology, Palaeoecology, v. 218, p. 15–56, doi: 10.1016/j.palaeo.2004.12.005.

Toro, B., and Pratt, B.R., 2015, Characteristics and implications of sedimentary deformation features in the Green River Formation (Eocene) in Utah and Colorado, in Vanden Berg, M.D., Resseter, R., and Birgenheier, L.P. eds., Geology of Utah's Uinta Basin and Uinta Mountains: Utah Geological Association Publication 44, p. 371–422.

Tucker, M.E., 2003, Mixed clastic-carbonate cycles and sequences; Quaternary of Egypt and Carboniferous of England: Geologia Croatica, v. 56, p. 19–37.

Tunbridge, I.P., 1984, Facies model for a sandy ephemeral stream and clay playa complex; the Middle Devonian Trentishoe Formation of North Devon, U.K.: Sedimentology, v. 31, p. 697–715.

Uba, C.E., Heubeck, C., and Hulka, C., 2005, Facies analysis and basin architecture of the Neogene Subandean synorogenic wedge, southern Bolivia: Sedimentary Geology, v. 180, p. 91–123.

Underwood Jr, J.R., and Lambert, W., 1974, Centroclinal cross strata, a distinctive sedimentary structure: Journal of Sedimentary Petrology, v. 44, p. 1111–1113, doi: 10.1029/WR014i006p01141.

Vanden Berg, M.D., 2008, Basin-wide evaluation of the uppermost Green River Formation's oil-shale resource, Uinta Basin, Utah and Colorado: Utah Geological Survey, v. 128, 19 p.

Vanden Berg, M.D., Lehle, D.R., Carne, S.M., Morgan, C.D., 2013, Geological characterization of the Birds Nest Aquifer, Uinta Basin, Utah – Assessment of the aquifer's potential as a saline water disposal unit: Utah Geological Survey Special Study 147, 57 p.

Vanden Berg, M.D., and Birgenheier, L.P., accepted, An examination of the saline phases of Eocene Lake Uinta, Upper Green River Formation, Uinta Basin, Utah: Journal of Paleolimnology.

Wang, B., and Ding, Q., 2008, Global monsoon: Dominant mode of annual variation in the tropics: Dynamics of Atmospheres and Oceans, v. 44, p. 165–183, doi: 10.1016/j.dynatmoce.2007.05.002.

White, M.A., and Jacobson, M.I., 1983, Structures associated with the southwest margin of the ancestral Uncompahgre Uplift: Grand Junction Geological Society Northern Paradox Basin – Uncompahgre Uplift Field Trip Guide, p. 33–39.

Wright, L.D., and Friedrichs, C.T., 2006, Gravity-driven sediment transport on continental shelves : A status report: Continental Shelf Research, v. 26, p. 2092–2107, doi: 10.1016/j.csr.2006.07.008.

Zachos, J.C., Pagani, M., Sloan, L.C., Thomas, E., and Billups, K., 2001, Trends, rhythms, and aberrations in global climate 65 Ma to present: Science, v. 292, p. 686–693, doi: 10.1126/science.1059412.

Zachos, J.C., Mccarren, H., Murphy, B., Röhl, U., and Westerhold, T., 2010, Tempo and scale of late Paleocene and early Eocene carbon isotope cycles : Implications for the origin of hyperthermals: Earth and Planetary Science Letters, v. 299, p. 242–249, doi: 10.1016/j.epsl.2010.09.004.

Zhisheng, A., Guoxiong, W., Jianping, L., Youbin, S., Yimin, L., Weijian, Z., Yanjun, C., Anmin, D., Li, L., Jiangyu, M., Hai, C., Zhengguo, S., Liangcheng, T., Hong, Y.,

et al., 2015, Global Monsoon Dynamics and Climate Change: Annu. Rev. Earth Planet. Sci, v. 43, p. 29–77, doi: 10.1146/annurev-earth-060313-054623.